Ma *et al. Satellite Navigation* (2024) 5:4
https://doi.org/10.1186/s43020-023-00124-3

Satellite Navigation
https://satellite-navigation.springeropen.com/

ORIGINAL ARTICLE Open Access

A rigorous real-time acoustic positioning method for ocean bottom seismic exploration

Jinye Ma[1,2], Shouchuan Fang[3*] and Jianhu Zhao[1,2]

Abstract

The conventional technique for positioning seafloor geophones in ocean bottom seismic exploration encounters several challenges, including the significant impact of outliers on positioning results, underutilization of high-precision observations, and low efficiency in real-time data processing. These issues inevitably affect the quality of seismic exploration outcomes. To address these challenges and enhance the accuracy of geophone positioning, this paper proposes a rigorous real-time acoustic positioning method for geophones based on sequential adjustment and Baarda's outlier detection approach. The proposed method comprises three key steps: grouping the original acoustic observations, constructing the intra-group acoustic positioning model, and synthesizing the positioning results across the different groups. The validity and practicality of this approach are confirmed through a simulation experiment as well as the field experiment conducted in the Bohai Sea, China. The results demonstrate that the proposed method effectively eliminates outliers in the original observations and maximizes the utilization of high-quality observations. Compared to traditional acoustic positioning methods, it significantly reduces positioning errors from meters to decimeters, and in some cases can achieve centimeter-level precision. When the sound velocity profile in the operating sea area is measured, the method can attain the posterior standard deviation at the millimeter level and positioning errors within 10 cm. When the sound velocity profile is unknown, the method can achieve the posterior standard deviation at centimeter-level and positioning errors of approximately 20 cm.

Keywords Ocean bottom seismic exploration, Geophone positioning, Acoustic positioning method, Sequential adjustment, Outlier detection

Introduction

Ocean bottom seismic exploration is a pivotal technology for the exploration and exploitation of deep-sea petroleum and natural gas resources. It mainly includes Ocean Bottom Cable (OBC) seismic exploration and Ocean Bottom Node (OBN) seismic exploration (Barr et al., 1996; Berg et al., 1994; Bovet et al., 2010; Lecerf et al., 2011).

In OBC seismic exploration, a cable embedded with seismic geophones is initially deployed onto the ocean floor. Subsequently, a gun array, consisting of multiple air guns, is towed by a survey ship to generate high-pressure gas and artificial seismic waves. The seismic data collected by the seafloor geophones are then analyzed to discern the submarine formation structure of the surveyed area, thereby determining the optimal location for oil and gas resource storage (Fang, 2014; Zinn, 1998). The principle underlying OBN seismic exploration is essentially identical to that of OBC seismic exploration, with the difference that OBN employs independent geophones connected by external cables (Alghamdi et al., 2018; Detomo et al., 2012; Zhang et al., 2021).

Accurate positioning of geophones plays a crucial role in determining the quality results of ocean bottom

*Correspondence:
Shouchuan Fang
lan816@sina.com
[1] School of Geodesy and Geomatics, Wuhan University, 129 Luoyu Road, Wuhan 430079, China
[2] Institute of Marine Science and Technology, Wuhan University, Wuhan 430079, China
[3] Surveying Service Center, BGP Inc., CNPC, Zhuozhou 072751, Hebei, China

seismic surveys. Due to the influence of oceanic factors such as waves, tides, and currents, the actual coordinates of the seafloor geophones often deviate significantly from the intended coordinates. Therefore, it is necessary to determine the precise coordinates of geophones after cable deployment to ensure the high quality of the ocean bottom seismic exploration results (Morvan et al., 2015; Wang et al., 2020; Zeng & Yang, 2001). There are three common techniques for geophone positioning. The first approach is recording and using the horizontal coordinates of the ship-borne GNSS antenna at the moment when geophones are dropped on the seafloor. The second method is attaching high-frequency acoustic transponders to the geophones and conducting a separate pinging survey for positioning purposes (acoustic positioning). The third technique is utilizing multiple occasions of the onset of seismic energy as surveying observations in a positioning algorithm (first breaks). It is also possible to combine acoustic positioning with first breaks (Zinn, 2011). The first method is the simplest one but provides the results with low accuracy.

Acoustic positioning has many advantages. It can be successfully utilized in the circumstances such as shallow water and shorelines, where the seismic shooting geometry may not allow for the balanced coverage required in the first break method (Bole & Zinn, 1998). Therefore, it has been widely integrated into seismic exploration software developed in different countries, such as the TZ/OBC acoustic positioning system of Sonardyne and the BPS acoustic positioning system of Bureau of Geophysical Prospecting, China National Petroleum Corporation (BGP INC., 2016; Sonardyne, 2021). The principle of acoustic positioning can be summarized as follows. Firstly, the one-way propagation time of the acoustic wave from the ship-borne acoustic transducer to the acoustic transponders installed on the seafloor geophones is recorded. Subsequently, the geometric distances between the transducer and transponders are calculated, and the coordinates of the transponders can be determined using the range intersection positioning model (Fujita et al., 2006; Zhao et al., 2018a, 2018b). Based on the above principles, acoustic positioning encounters several challenges in data processing.

Firstly, the positioning accuracy of a geophone is contingent upon the accuracy of acoustic ranging. The acoustic propagation path undergoes bending due to the change of sound velocity in seawater, resulting in a discrepancy between the actual geometric distance and the geometric distance calculated using the one-way propagation time and the sound velocity on the sea surface. High-precision acoustic ranging results can be obtained by acoustic ray tracing, such as acoustic ray tracing under the assumption of constant sound velocity in the layer and the assumption of the constant gradient of sound velocity in the layer (Medwin & Clay, 1998; Sakic et al., 2018). However, the accuracy of acoustic ray tracing is related to the sampling interval of the Sound Velocity Profile (SVP). Smaller sampling intervals lead to higher tracing accuracy. Nevertheless, measuring the SVP requires the vessel to be in a fixed position and necessitates multiple sound velocity samples in the water area because the underwater sound velocity varies in both vertical and horizontal directions in time, which is time-consuming and labor-intensive (Bianco & Gerstoft, 2017; Clarke et al., 2000). Considering the operational efficiency and cost, SVPs are rarely measured in ocean bottom seismic exploration. Therefore, it becomes imperative to study the method for processing acoustic positioning data without SVPs. At present, the main method to solve this problem is to use the historical SVPs in the area to derive the SVP at the time of operation. Munk and Wunsch (1979) proposed the idea of ocean acoustic tomography. They studied the relationship between the propagation time disturbance and the change of sound velocity in the water and retrieved the sound velocity field in the water by repeatedly measuring the propagation time of sound waves between the sound source and the transponder. Leblanc et al. (1980) proposed the method of using Empirical Orthogonal Function (EOF) to analyze SVPs, whose effectiveness was proved by many scholars through the experiments in different time and sea areas (Ding et al., 2007; Huang et al., 2021; LeBlanc & Middleton, 1980; Park & Kennedy, 1996; Sun et al., 2016). Based on the empirical relationship between sound velocity and water temperature, Osada et al. (2003) obtained accurate three-dimensional horizontal coordinates and sound velocity field of the seafloor transponder with the constraint of the horizontal coordinates. However, in the geophone positioning, the real coordinates of the seafloor geophone differ greatly from the design coordinates and cannot be used as the constraint conditions. Li et al. (2015) found the optimal solution of the optimal sound velocity through the grid search algorithm to inverse the SVP with the difference between the theoretical spectrum and the observed spectrum of the acoustic signal as the constraint condition. Zhao et al. (2023) proposed a SVP inversion method under the self-constraint of water depth. Combining the initial SVP calculated by Argo observation data, the simulated annealing algorithm was used for SVP inversion. The above methods of sound velocity inversion require constraints such as historical observations of SVPs, relatively accurate coordinates, real terrain, or Argo observation data, etc. However, meeting these conditions is often challenging in seismic exploration geophone positioning. Therefore, it is necessary to further study the method of

geophone positioning without additional data such as historical SVPs.

The second challenge lies in the underutilization of high-quality acoustic observations. During the ocean bottom seismic exploration, the survey ship travels along a predetermined trajectory while collecting acoustic observations between the ship-borne transducer and the transponder on the geophone (Barr, 1994). As the geophone enters or is about to depart from the effective range of the survey vessel, the incident angle of the acoustic wave becomes exceedingly large, reducing the accuracy of the acoustic ranging. As the survey ship approaches the geophone, the incident angle gradually decreases and the accuracy of acoustic ranging is gradually improved (Zhao & Liang, 2019). Currently, in establishing the acoustic positioning model, all observations from the current moment and the past are incorporated without discerning their quality, resulting in the suboptimal utilization of high-quality observations and significant wastage of data. Therefore, it is of great significance to study the processing scheme of acoustic observations under different incident angles to enhance the positioning accuracy of the geophone. To solve this problem, Wang et al. (2016) used the curvature radius of the sound propagation path to replace the Snell constant in the process of ray tracing when the incidence angle is too large. This method is more accurate than the traditional method when the incidence angle is greater than 80 degrees. Zhao et al., (2018a, 2018b) constructed four kinds of underwater positioning random models based on the incidence angle of sound waves: the general proportional weighting model, the cosine weighting model, the exponential weighting model, and the piecewise-cosine weighting model. Wang et al. (2021) built a piecewise exponential function stochastic model based on the constant gradient acoustic ray tracing, whose positioning results are more precise than the traditional acoustic positioning method and the same as the piecewise-cosine weighting model. All the above methods need to incorporate all the observed data into the positioning model and then determine their weights, which is suitable for post-processing the data rather than real-time. Based on these studies, this paper will further study the stochastic model suitable for the real-time positioning model of geophones.

The third problem is the insufficient robustness of the basic acoustic positioning model. The basic acoustic positioning model based on the classical least squares cannot distinguish outliers in the observations, and its positioning results are greatly affected by abnormal observations (Wang et al., 2014). Therefore, it is very important to explore the acoustic positioning model that incorporates outlier elimination functionality to improve the positioning accuracy of the geophone. Currently, two commonly employed methods for outlier removal are Baarda's outlier detection approach and the IGGI method (Baarda, 1967, 1968; Li et al., 2004). Baarda's method only requires a single critical value, making it more convenient to implement compared to IGGI, which necessitates a trimmed parameter and two threshold values (Li et al., 2022). As a result, Baarda's method proves to be more user-friendly. The outlier detection based on Baarda's theory typically identifies one outlier at a time, with the overall set of outliers generally determined through an iterative process.

In summary, addressing the issues of the absence of the SVP, underutilization of high-quality acoustic observations, and inadequate robustness of acoustic positioning model in the acoustic positioning of geophones, this paper proposed a rigorous real-time acoustic positioning method for seafloor geophones. The subsequent sections of this paper are structured as follows. Sect. 2 provides a concise introduction to the principle of acoustic positioning. Section 3 elaborates on the specific details of the proposed rigorous real-time positioning method for geophones, mainly including the grouping strategy of acoustic observations, the establishment of the intra-group acoustic positioning model, the elimination of outliers in the intra-group acoustic observations and the synthesis of geophone positioning results between groups. Section 4 verifies the practicality and accuracy of this proposed method through simulation and field experiments. Section 5 discusses the optimal applicable conditions of the proposed method. Finally, the conclusion highlights the contribution of this paper.

The basic acoustic positioning model for seafloor geophones

The acoustic positioning system is a ranging positioning system. As depicted in Fig. 1, when the acoustic signal emitted from a ship-borne acoustic transducer is received by the acoustic transponder mounted on the seafloor geophone, the coordinates of the ship-borne transducer, the commencement time of signal transmission, and the time of signal reception are meticulously recorded.

Let $t_{i,0}$ denote the emission time of the i-th acoustic wave, and $t_{i,m}$ be the time when the m-th geophone receives the signal. If the velocity c of the acoustic wave propagating in water is measured, then the distance $S_{i,m}$ between the ship-borne transducer and the m-th geophone can be calculated, and the observation equation is shown in Eq. (1).

$$\begin{aligned} S_{i,m} &= c\left(t_{i,m} - t_{i,0}\right) \\ &= \sqrt{(X_m - X_i)^2 + (Y_m - Y_i)^2 + (Z_m - Z_i)^2} + \varepsilon_{i,m} \end{aligned} \tag{1}$$

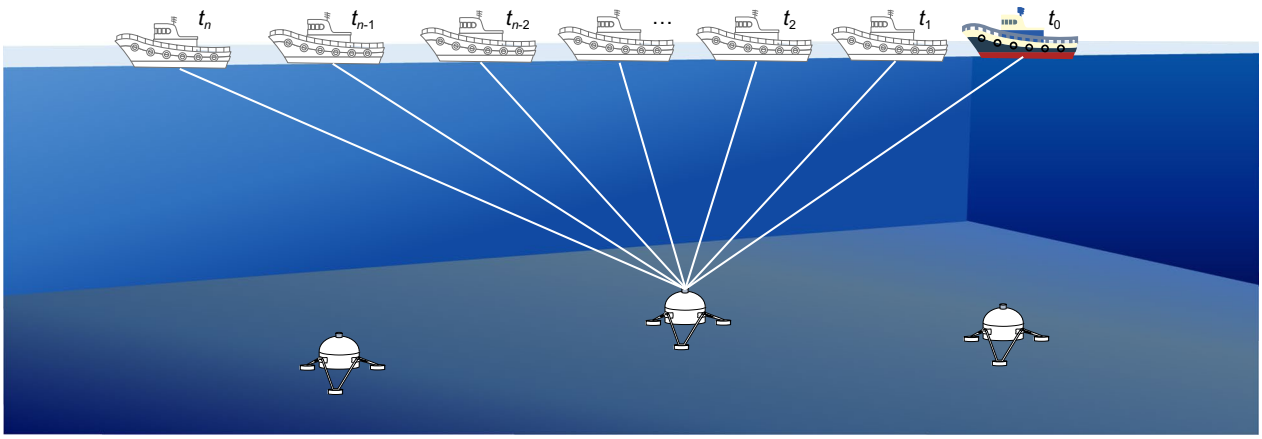

Fig. 1 The basic principle of acoustic positioning with the white ship icon indicating the positions of the survey ship at different time

where (X_i, Y_i, Z_i) and (X_m, Y_m, Z_m) represent the coordinates of the ship-borne transducer and the m-th geophone at the i-th observation epoch, respectively, and $\varepsilon_{i,m}$ is the observation error.

Drawing upon Taylor's theorem, the linearization error equation can be expressed as Eq. (2).

$$v_{i,m} = a_{i,1}\mathrm{d}x + a_{i,2}\mathrm{d}y + a_{i,3}\mathrm{d}z - \left(S_{i,m} - S^0_{i,m}\right) \tag{2}$$

where $S^0_{i,m}$ is the geometric distance calculated by the coordinates of the ship-borne transducer at the i-th observation epoch with the approximate coordinates (X^0_m, Y^0_m, Z^0_m) of the m-th geophone. The precise expression form of each parameter in the above formula is shown in Eq. (3).

$$\begin{cases} a_{i,1} = \dfrac{X_i - X^0_m}{S^0_{i,m}}, \quad a_{i,2} = \dfrac{Y_i - Y^0_m}{S^0_{i,m}}, \quad a_{i,3} = \dfrac{Z_i - Z^0_m}{S^0_{i,m}} \\ S^0_{i,m} = \sqrt{\left(X_i - X^0_m\right)^2 + \left(Y_i - Y^0_m\right)^2 + \left(Z_i - Z^0_m\right)^2} \end{cases} \tag{3}$$

All the error equations in Eq. (2) corresponding to the m-th geophone can be arranged in matrix form as follows:

$$\boldsymbol{V}_m = \boldsymbol{B}_m \hat{\boldsymbol{x}}_m - \boldsymbol{l}_m \tag{4}$$

Based on the least-squares criterion $\boldsymbol{V}^{\mathrm{T}}\boldsymbol{P}\boldsymbol{V} = \min$, the coordinate correction vector $\hat{\boldsymbol{x}}_{\boldsymbol{m}}$ can be estimated by Eq. (5):

$$\hat{\boldsymbol{x}}_m = \left(\boldsymbol{B}^T_m \boldsymbol{P}_m \boldsymbol{B}_m\right)^{-1} \boldsymbol{B}^T_m \boldsymbol{P}_m \boldsymbol{l}_m \tag{5}$$

where $\boldsymbol{P}_{\boldsymbol{m}}$ represents the weight matrix, which is a diagonal matrix with the diagonal elements determined according to the accuracy of acoustic observations. Then, the coordinates $\boldsymbol{X}_{\boldsymbol{m}}$ of the m-th geophone can be calculated by Eq. (6).

$$\boldsymbol{X}_m = \boldsymbol{X}^0_m + \hat{\boldsymbol{x}}_m \tag{6}$$

In the derivation process of Eqs. (1)–(2), the approximate coordinates of the geophone are used to linearize the original observation equation, and the higher order term of the linearized observation equation is abandoned, which loses part of the accuracy of the acoustic observation value. If the approximate coordinates of the geophone differ greatly from the real coordinates, the accuracy of the final coordinates will be affected. Iteratively solving the coordinates of the geophone can reduce the influence of inaccurate approximate coordinates on the final positioning results. The solution process is as follows. Add the coordinate correction values obtained by Eq. (5) to the original approximate coordinates X^0_m as the new approximate coordinates; Reconstruct the basic acoustic positioning model by repeating Eqs. (2)–(4); Re-solve the coordinate correction vector based on Eq. (5); Stop iteration when the corresponding difference of each element in the coordinate correction vector in the solution of two adjacent iterations is less than the set threshold; Finally, the coordinates of the geophone can be calculated by combining the approximate coordinates and the coordinate correction values in the last iteration.

The posterior standard deviation σ_0 of the basic acoustic positioning model, the variance matrix $\boldsymbol{D}_{\hat{x}\hat{x}}$ and the covariance matrix $\boldsymbol{Q}_{\hat{x}\hat{x}}$ of $\hat{\boldsymbol{x}}_{\boldsymbol{m}}$ are given in Eq. (7).

$$\begin{cases} \sigma_0 = \sqrt{\boldsymbol{V}_m^T \boldsymbol{P}_m \boldsymbol{V}_m \Big/ (n-3)} \\ \boldsymbol{Q}_{\hat{x}\hat{x}} = \left(\boldsymbol{B}_m^T \boldsymbol{P}_m \boldsymbol{B}_m\right)^{-1} \\ \boldsymbol{D}_{\hat{x}\hat{x}} = \sigma_0^2 \boldsymbol{Q}_{\hat{x}\hat{x}} \end{cases} \tag{7}$$

Once the geophone enters the effective operating range of the survey ship, the propagation time of the acoustic signal from the ship-borne transducer to the geophone is collected. When the number of observations exceeds three, the positioning model depicted in Eq. (4) can be constructed to calculate the real-time coordinates of the geophone.

The rigorous real-time positioning method for geophones

There are three problems in the basic acoustic positioning of geophones: (1) The acoustic positioning model is seriously influenced by the outliers in the observations; (2) The observation values at all observation epochs are encompassed in the model, without discerning the quality of the large amount of observations; (3) The need to retain the initial observation value from each epoch hampers computational efficiency and imposes significant memory pressure. To solve the above problems, this paper proposes a rigorous real-time acoustic positioning method for geophones based on sequential adjustment, named the Sequential acoustic positioning method (called "the SQ acoustic positioning method" for short).

As shown in Fig. 2, the flow of the SQ acoustic positioning method is as follows. Firstly, the acoustic observations collected during the survey are grouped. Subsequently, the intra-group acoustic positioning model is established to solve the coordinates of geophones using the observations in the same group considering whether the SVP in the area is measured or not, and Baarda's outlier detection is iteratively employed to eliminate outliers. Finally, the sequential adjustment is used to synthesize the positioning results of each group.

The grouping strategy of original acoustic observations

According to Fig. 2, before establishing the intra-group acoustic positioning model, it is necessary to collect acoustic observations in groups, which is performed in real-time during the navigation of the survey ship. The accuracy of acoustic ranging diminishes as the incident angle of the acoustic waves increases. Therefore, to ensure the consistent quality of the observations within the same group, it is advisable to adjust the data buffer size based on the velocity of the survey ship. If the speed of the ship is too fast, the data buffer size ought to be reduced; conversely, if the speed of the ship is too low, the data buffer size should be increased (Fig. 3).

The survey ship continuously collects acoustic observations and monitors the capacity of the data buffer. Once the buffer reaches its maximum capacity, the data collection for that group is concluded. Simultaneously, the buffer is cleared for the next set of data collection.

The establishment of the intra-group acoustic positioning model

After the data collection for a group is concluded, the positioning model is constructed within the group to calculate the coordinates of geophones. The construction of the intra-group acoustic positioning model bears resemblance to the methodology outlined in Sect. 2. This section will introduce distinct weighting methods for acoustic observations.

(1) The weighting strategy for acoustic observations when the SVP is known.

When the SVP is known, the initial incidence angle of the acoustic wave can be calculated by combining the one-way propagation time with the SVP. Then the geometric distance between the onboard transducer and geophones can be determined through acoustic ray tracing. In this case, the observations can be weighted based on the magnitude of the geometric distance, assigning smaller weights to longer distances. At present, the commonly employed acoustic ray tracing methods include the tracing under the assumption of constant sound velocity in the same layer and the tracing under the assumption of the constant gradient of sound velocity in the same water layer.

Assuming that the acoustic wave passes through a water column consisting of n layers, with the sound velocity at the sea surface denoted as C_0, and the initial incident angle as θ_0; the i-th layer has a thickness of Δz_i, a sound velocity of C_i, and an incident angle of θ_i. Then the horizontal displacement Δy_i and propagation time Δt_i in the i-th layer calculated by the ray tracing under the assumption of constant sound velocity are given in Eq. (8).

$$\begin{cases} \Delta t_i = \dfrac{\Delta z_i}{C_i \cos\theta_i} = \dfrac{\Delta z_i}{C_i \sqrt{1-(pC_i)^2}} \\ \Delta y_i = \Delta z_i \tan\theta_i = \dfrac{\Delta z_i C_i p}{\sqrt{1-(pC_i)^2}} \end{cases} \tag{8}$$

where p is a constant and satisfies the Snell law given by Eq. (9).

$$\frac{\sin\theta_0}{C_0} = \frac{\sin\theta_i}{C_i} = \frac{\sin\theta_{i+1}}{C_{i+1}} = p \tag{9}$$

Based on Eq. (8), the total propagation time t_i, the total horizontal displacement y_i and the depth displacement

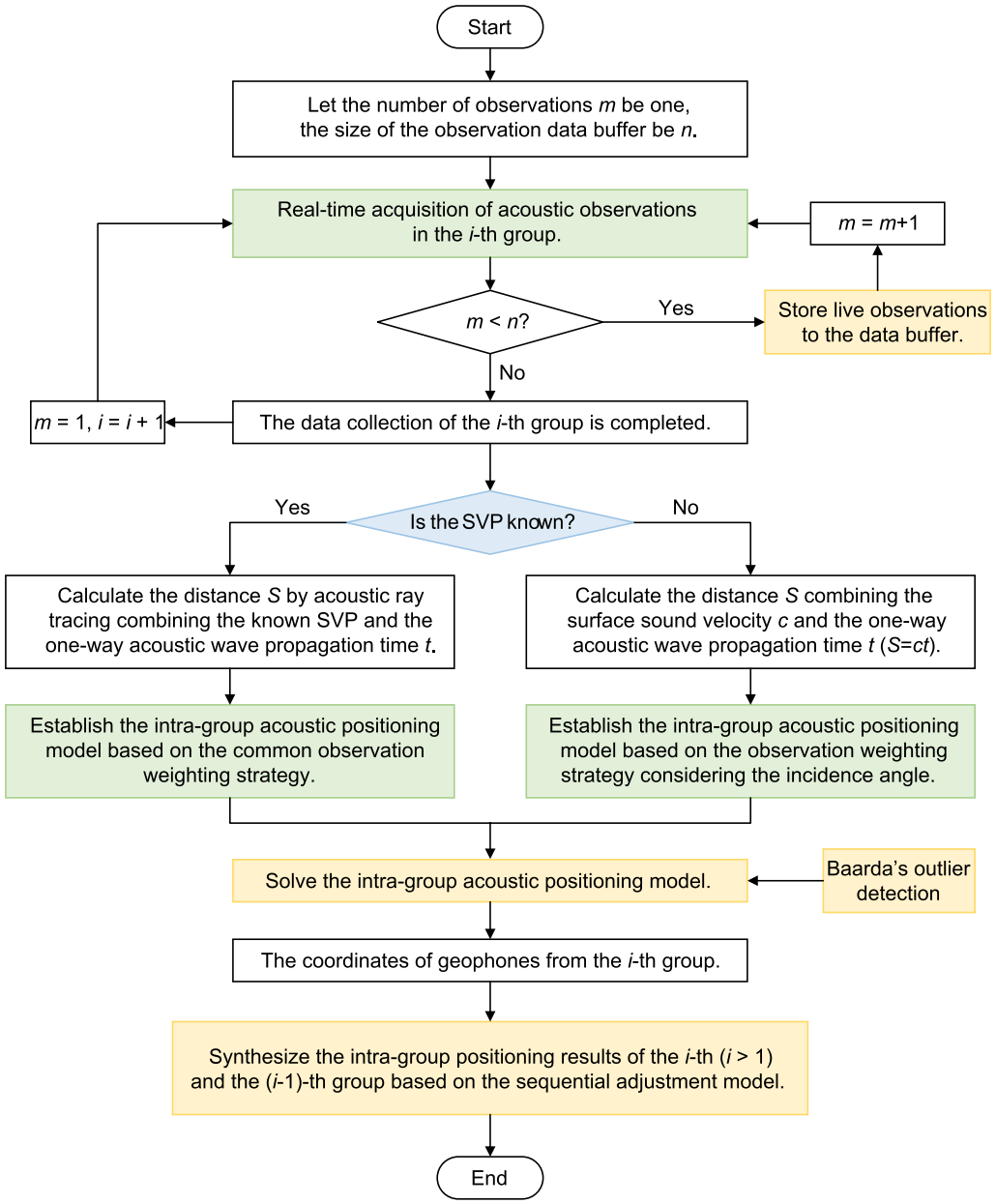

Fig. 2 The flow chart of the SQ acoustic positioning method

z_i of the sound wave after passing through the i-th water layer are given as follows:

$$t_i = \sum_{k=1}^{i} \Delta t_k, y_i = \sum_{k=1}^{i} \Delta y_k, z_i = \sum_{k=1}^{i} \Delta z_k \tag{10}$$

Determine whether the acoustic ray tracing should be finished is based on the observed one-way propagation time T. When t_i is less than T, the acoustic ray tracing of the next layer should be continued. When t_i is greater than T, stop the acoustic ray tracing and check whether there exists over-tracing. If t_i is still less than T after the acoustic ray tracing in each water layer is completed, the horizontal and vertical displacements for the missing time should be complemented based on the sound velocity of the last water layer. Once the acoustic ray tracing is completed, the geometric distance $S_{j,m}$ between the ship-borne transducer at the j-th observation epoch and the m-th geophone can be obtained with Eq. (11):

$$S_{j,m} = \sqrt{y^2 + z^2} \tag{11}$$

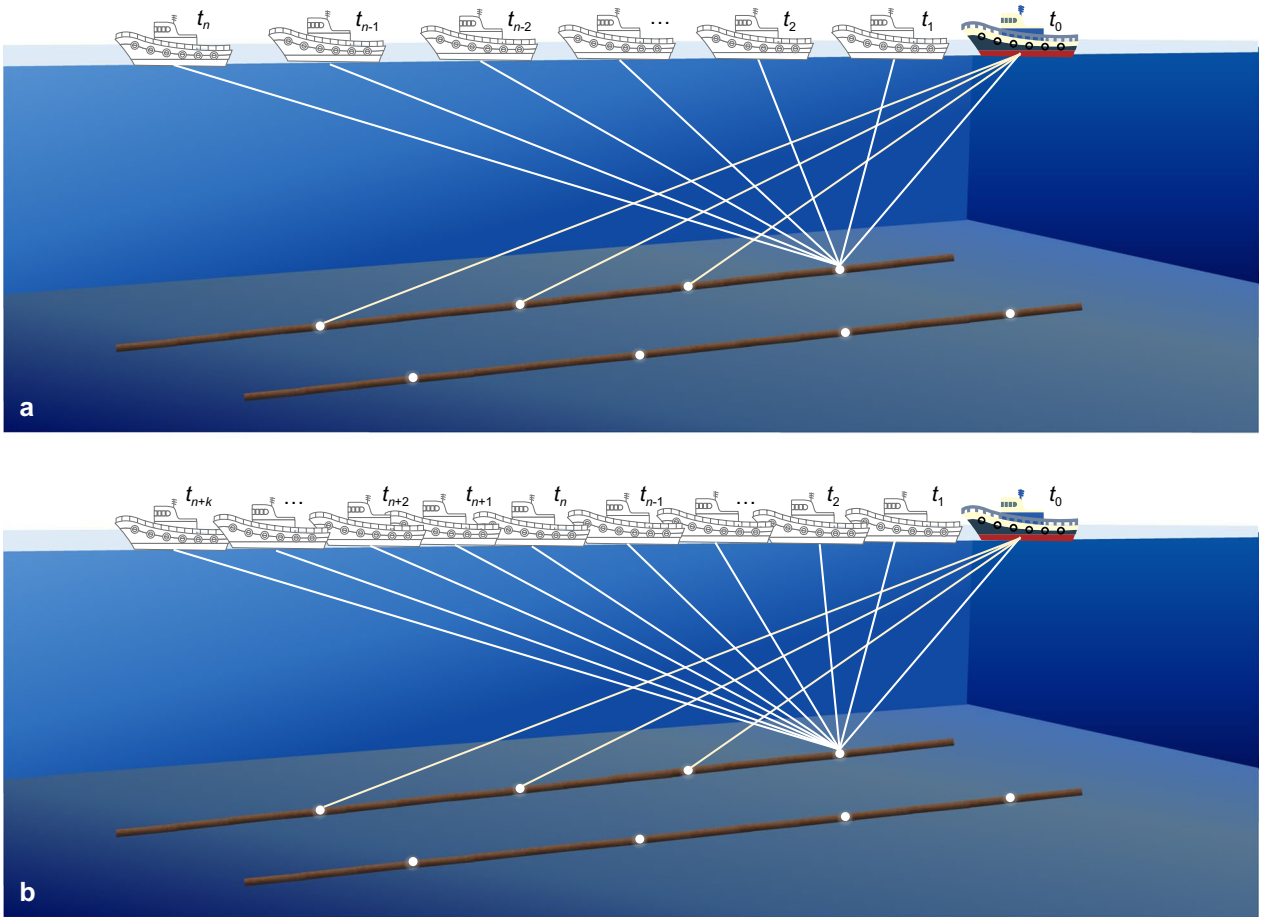

Fig. 3 The data buffer size setting of different ship speeds under the same geometric structure, where the glowing white dot indicates the geophone. **a** The speed of the surveying ship is fast; **b** The speed of the surveying ship is slow

where y and z are the total horizontal and depth displacements of the sound wave at the j-th observation epoch. Finally, the distance observation can be weighted according to Eq. (12).

$$P_j = 1/S_{j,m} \tag{12}$$

(2) The weighting strategy for acoustic observations when the SVP is unknown.

Considering the efficiency and cost, the SVP is rarely collected in the ocean bottom seismic exploration. Consequently, the distance between the ship-borne transducer and the geophone, calculated by multiplying the sound velocity on the sea surface by the one-way propagation time of the acoustic wave, deviates significantly from the actual value. Therefore, it is necessary to redefine the weighting strategy for acoustic observations. By differentiating the second and third equations in Eq. (10), we can derive the following formula:

$$\begin{cases} dy = d\left(\sum_{i=1}^{n}\Delta y_i\right) = \sum_{i=1}^{n}\tan\theta_i d(\Delta z_i) + \sum_{i=1}^{n}\dfrac{\Delta z_i d\theta_i}{\cos^2\theta_i} \\ dz = d\left(\sum_{i=1}^{n}\Delta z_i\right) = \sum_{i=1}^{n} d(\Delta z_i) \end{cases} \tag{13}$$

By differentiating Eqs. (9), (14) can be obtained.

$$d\theta_i = \frac{C_i\cos\theta_0}{C_0\cos\theta_i}d\theta_0 \tag{14}$$

By combining Eq. (13) and Eq. (14), the relation between the accuracy of acoustic ranging σ_S and the accuracy of the initial incidence angle σ_{θ_0} can be obtained based on the law of variance propagation, as shown in Eq. (15). The detailed derivation process is given in the Appendix.

$$\sigma_S = \frac{yC_0^2 \cos\theta_0}{\sqrt{y^2+z^2}} \left(\sum_{i=1}^{n} \frac{\Delta z_i C_i}{\sqrt{\left(C_0^2 - C_i^2 \sin^2\theta_0\right)^3}} \right) \sigma_{\theta_0} \tag{15}$$

In the ocean bottom seismic survey, the SVP is unknown, which means the distance observations are directly calculated by multiplying the surface sound velocity C_0 and the one-way propagation time of acoustic wave. The following formula exists:

$$\begin{cases} C_i = C_0 \\ \sin\theta_i = \sin\theta_0 \end{cases} \tag{16}$$

Substituting the above formula into Eq. (15), we can obtain the following formula:

$$\sigma_S = (z \tan\theta_0 \sec\theta_0)\sigma_{\theta_0} \tag{17}$$

Based on Eq. (17), the weighting strategy for distance observations can be derived in the absence of SVPs. Firstly, set the acoustic ranging accuracy of an initial incident angle whose acoustic ranging error is small as the reference value. Then, the weight of distance observations at the j-th observation epoch can be calculated by Eq. (18):

$$P_j = \frac{z_{ref}^2 \tan^2\theta_0^{ref} \sec^2\theta_0^{ref}}{z_j^2 \tan^2\theta_0^j \sec^2\theta_0^j} \tag{18}$$

where θ_0^{ref} and θ_j^0 are the initial incident angles corresponding to the reference observation and the j-th observation, obtained by Eq. (19), respectively, and z_{ref} and z_j are the water depths corresponding to the reference observation and the j-th observation, respectively.

$$\theta_0^j = \arctan\left(\frac{\sqrt{\left(X_j - X_m^0\right)^2 + \left(Y_j - Y_m^0\right)^2}}{Z_j - Z_m^0} \right) \tag{19}$$

In Eq. (19), (X_j, Y_j, Z_j) are the coordinates of the ship-borne transducer at the j-th observation epoch and (X_m^0, Y_m^0, Z_m^0) are the approximate coordinates of the m-th seafloor geophones.

Equation (18) gives the weighting method for acoustic observations when the SVP is unknown. At present, there are some weighting methods based on the incident angle of sound waves, most of which are functions of the initial incidence angle of sound waves, and the model parameters need to be solved from the known observed values. Therefore, compared with the existing weighting method based on the incidence angle of sound waves, the proposed method is simpler and more suitable for real-time data processing.

The outlier elimination of acoustic observations

Baarda's outlier detection method is adopted to iteratively identify and remove outliers in the process of solving the intra-group acoustic positioning model. The flow chart of this process is presented in Fig. 4. After solving the intra-group acoustic positioning model, the n-dimensional correction vector $\boldsymbol{V}$ of the observations and its covariance matrix $\boldsymbol{Q}_{vv}$ can be obtained, as shown in Eq. (20).

$$\boldsymbol{Q}_{vv} = \boldsymbol{P}^{-1} - \boldsymbol{B}\left(\boldsymbol{B}^T\boldsymbol{P}\boldsymbol{B}\right)^{-1}\boldsymbol{B}^T \tag{20}$$

where $\boldsymbol{P}$ represents the weight matrix of the acoustic observations within the same group, matrix $\boldsymbol{B}$ has the same meaning in Eq. (7).

Denote the element of $\boldsymbol{Q}_{\mathrm{vv}}$ in row i and column i as $Q_{v_iv_i}$. Given the null hypothesis H_0: $\mathrm{E}(v_i)=0$, indicating the absence of outliers within the group, and considering v_i follows the normal distribution with variance $\sigma_0^2 Q_{v_iv_i}$, the standard normal distribution statistic shown in Eq. (21) can be constructed.

$$u_i = \frac{|v_i|}{\sigma_0\sqrt{Q_{v_iv_i}}} = \frac{|v_i|}{\sigma_{v_i}} \tag{21}$$

With significant level α, if u_i is greater than $u_{\alpha/2}$, the null hypothesis H_0 is rejected, which means the i-th acoustic observation L_i is an outlier and should be eliminated. Then continue to detect whether the next observation is an outlier until all observations have been detected.

The synthesis of acoustic positioning results between groups

The final step of the SQ acoustic positioning method is to synthesize the acoustic positioning results of different groups through sequential adjustment. Let $\boldsymbol{L_{i-1}}$ and $\boldsymbol{L_i}$ represent the acoustic observation vectors in the (i-1)-th and i-th periods, respectively, and their weight matrices are $\boldsymbol{P_{i-1}}$ and $\boldsymbol{P_i}$, as shown in Eq. (22), in which $\boldsymbol{O}$ is the zero matrix, the sizes of $\boldsymbol{P_{i-1}}$, $\boldsymbol{P_i}$ and $\boldsymbol{O}$ are determined by the number of observations.

$$\begin{cases} \boldsymbol{L} = \begin{pmatrix} \boldsymbol{L_{i-1}} \\ \boldsymbol{L_i} \end{pmatrix} \\ \boldsymbol{P} = \begin{pmatrix} \boldsymbol{P_{i-1}} & \boldsymbol{O} \\ \boldsymbol{O} & \boldsymbol{P_i} \end{pmatrix} \end{cases} \tag{22}$$

If there is no correlation between the observations, the error equations corresponding to the two periods can be expressed as the following equation:

$$\begin{cases} \boldsymbol{V_{i-1}} = \boldsymbol{B_{i-1}}\hat{\boldsymbol{x}} - \boldsymbol{l_{i-1}} \\ \boldsymbol{V_i} = \boldsymbol{B_i}\hat{\boldsymbol{x}} - \boldsymbol{l_i} \end{cases} \tag{23}$$

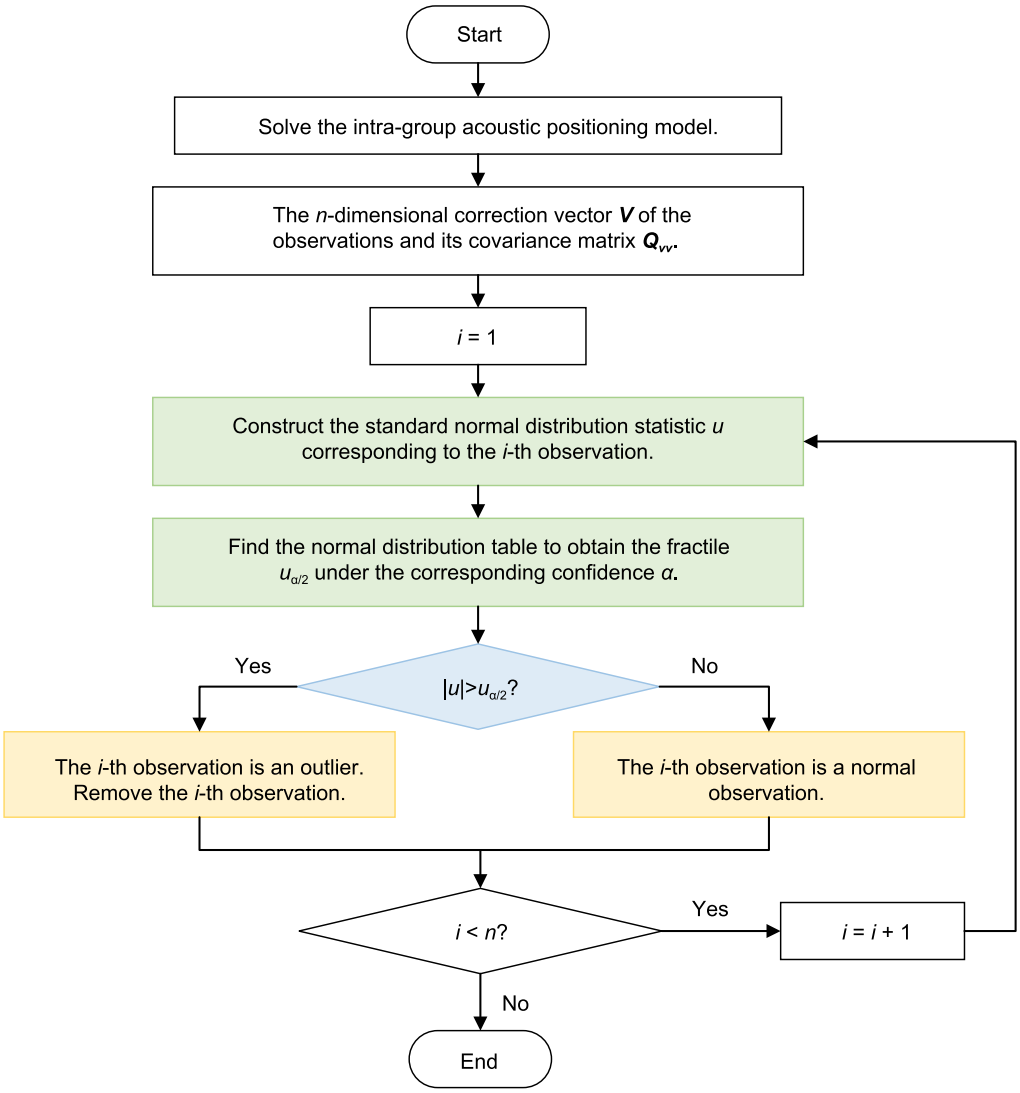

Fig. 4 The flow chart of eliminating outliers

where $\hat{\boldsymbol{X}} = \boldsymbol{X}_0 + \hat{x}$, $\boldsymbol{l_k} = \boldsymbol{L_k} - \boldsymbol{S_0^k}(k = i-1,\ i)$, $\boldsymbol{X_0}$ denotes the approximate coordinate vector of geophones, and S_0^k represents the distance vector between ship-borne transducer and geophones calculated based on $\boldsymbol{X_0}$. By solving the first formula in Eq. (23), we obtain the coordinate corrections of the (i-1)-th period $\hat{\boldsymbol{x}}_{\boldsymbol{i-1}}$, as shown in Eq. (24)

$$\hat{\boldsymbol{x}}_{i-1} = \left(\boldsymbol{B}_{i-1}^T \boldsymbol{P}_{i-1} \boldsymbol{B}_{i-1}\right)^{-1} \boldsymbol{B}_{i-1}^T \boldsymbol{P}_{i-1} \boldsymbol{l}_{i-1} \tag{24}$$

Let $\bar{\boldsymbol{l}}_i = \boldsymbol{l_i} - \boldsymbol{B_i}\hat{\boldsymbol{x}}_{i-1}$, then the coordinate correction vector of the i-th period can be given by Eq. (25) (Cui et al., 2015).

$$\hat{\boldsymbol{x}}_i = \left(\boldsymbol{B}_{i-1}^T \boldsymbol{P}_{i-1} \boldsymbol{B}_{i-1} + \boldsymbol{B}_i^T \boldsymbol{P}_i \boldsymbol{B}_i\right)^{-1} \boldsymbol{B}_i^T \boldsymbol{P}_i \bar{\boldsymbol{l}}_i \tag{25}$$

Subsequently, the coordinate vector of geophones, which combines the intra-group positioning results in the (i-1)-th and i-th periods can be given in Eq. (26).

$$\boldsymbol{X} = \boldsymbol{X}_0 + \hat{x}_{\boldsymbol{i}} \tag{26}$$

The comprehensive posterior standard deviation $\hat{\sigma}_0$ is given in Eq. (27), where n is the sum of the number of observations in the two periods and k is equal to three times the number of geophones.

$$\hat{\sigma}_0 = \sqrt{\left(\overline{\boldsymbol{V}}_{i-1}^T \boldsymbol{P}_{i-1} \overline{\boldsymbol{V}}_{i-1} + \hat{\boldsymbol{x}}_i^T \boldsymbol{P}_{i-1} \hat{\boldsymbol{x}}_i + \boldsymbol{V}_i^T \boldsymbol{P}_i \boldsymbol{V}_i\right)/(n-k)} \tag{27}$$

The specific calculation method of each parameter in the above formula is provided by Eq. (28).

$$\begin{cases} \overline{\boldsymbol{V}}_{i-1} = \boldsymbol{B}_{i-1}\hat{\boldsymbol{x}}_{i-1} - \boldsymbol{l}_{i-1} \\ \boldsymbol{V}_{\boldsymbol{i}} = \boldsymbol{B}_{\boldsymbol{i}}\hat{\boldsymbol{x}}_{\boldsymbol{i}} - \bar{\boldsymbol{l}}_{\boldsymbol{i}} \end{cases} \tag{28}$$

Since the observations under different incident angles have been distinguished when the observations are weighted, this method can reduce the influence of low-quality observations on high-quality ones, enhance calculation efficiency, and ensure optimal utilization of high-quality observations.

Experiment and analysis

To assess the practicability and accuracy of the proposed method, the simulation and field experiments are performed.

Simulation experiment

The simulation experiment is carried out first to test the effectiveness of the proposed method. Assuming the deployment of ten geophones at a water depth of 100 m with an approximate spacing of 50 m between adjacent geophones, and the design coordinates of the geophones are given in Table 1. Let the seismic survey ship go around geophones to conduct traveling observation, the two-dimensional track map is shown in Fig. 5a.

Utilizing the SVP depicted in Fig. 6b, in conjunction with the real-time coordinates of the ship-borne transducer and the actual coordinates of geophones, the inverse operation of acoustic ray tracing is employed to calculate the theoretical initial incidence angle and one-way propagation time for each observation epoch (Sakic et al., 2018, 2020). The results are given in Fig. 6.

Based on the initial incident angle and one-way propagation time of the sound wave obtained through the inverse operation of the acoustic ray tracing in Fig. 6, the acoustic ray tracing is performed again. The mean and standard deviation of the differences between the acoustic ray tracing results (vertical displacement ΔZ, horizontal displacement ΔD, and geometric distance ΔS) and the actual values are calculated, as in Table 2.

It can be seen from Table 2 that the difference between the geometric distance obtained by acoustic ray tracing and the actual value is within 5 cm. This disparity is attributed to the error in acoustic ray tracing and can be considered as an observation error during the field investigation. The methods given in Table 3 are employed to determine the coordinates of geophones.

In Table 3, "Basic" represents the basic acoustic positioning model and "SQ" represents the SQ acoustic positioning model. C_0 is the sound velocity on the sea surface. Acoustic observations include initial incidence angles of sound waves and geometric distances between the shipborne transducer and geophones. When the SVP is known, acoustic observations are calculated by ray tracing, otherwise, obtained based on Eq. (19). When the ratio of outliers exists, outliers equivalent to 5 percent of the total number of observations are introduced to the original acoustic observations. If Baarda's outlier detection method is used to remove outliers, the significant level α is set to 0.025 to achieve the 95% confidence level, and the critical value $u_{\alpha/2}$ is 1.96.

Figures 7, 8, and 9 show the differences between the geophone coordinates obtained by each method and the actual values in Table 1. Table 4 presents a posterior standard deviation (σ) of positioning models in method 1 to method 7. Table 5 gives the positioning errors (ΔP) in method 1 to method 7.

The following conclusions can be drawn from Table 4 and 5:

(1) When the SVP is known, both the basic acoustic positioning model in method 1 and the SQ positioning model in method 2 achieve accuracy at millimeter level. The coordinate differences between the positioning results with these two models and the actual values are approximately 10 cm. The reason for the smaller positioning error with the basic acoustic positioning model in method 1 than that with the SQ positioning model in method 2 is the greater number of redundancies in the former than that in the latter.

(2) When the SVP is unknown, the positioning accuracy of the basic acoustic positioning model in method 3 lowers to 20 cm. The coordinate differences between the positioning results and the actual values reach the meter level, especially in the depth direction. On the other hand, the SQ posi-

Table 1 The coordinates of geophones in the simulation experiment. The letter "*N*", "*E*" and "*U*" represent the north, east and depth direction

Point name	*N* (m)	*E* (m)	*U* (m)
G1	− 250.026	0.078	− 100
G2	− 199.834	− 0.045	− 100
G3	− 150.183	0.147	− 100
G4	− 100.155	− 0.060	− 100
G5	− 50.119	0.093	− 100
G6	0.159	− 0.196	− 100
G7	49.840	− 0.014	− 100
G8	99.868	0.173	− 100
G9	149.937	0.100	− 100
G10	199.984	0.115	− 100

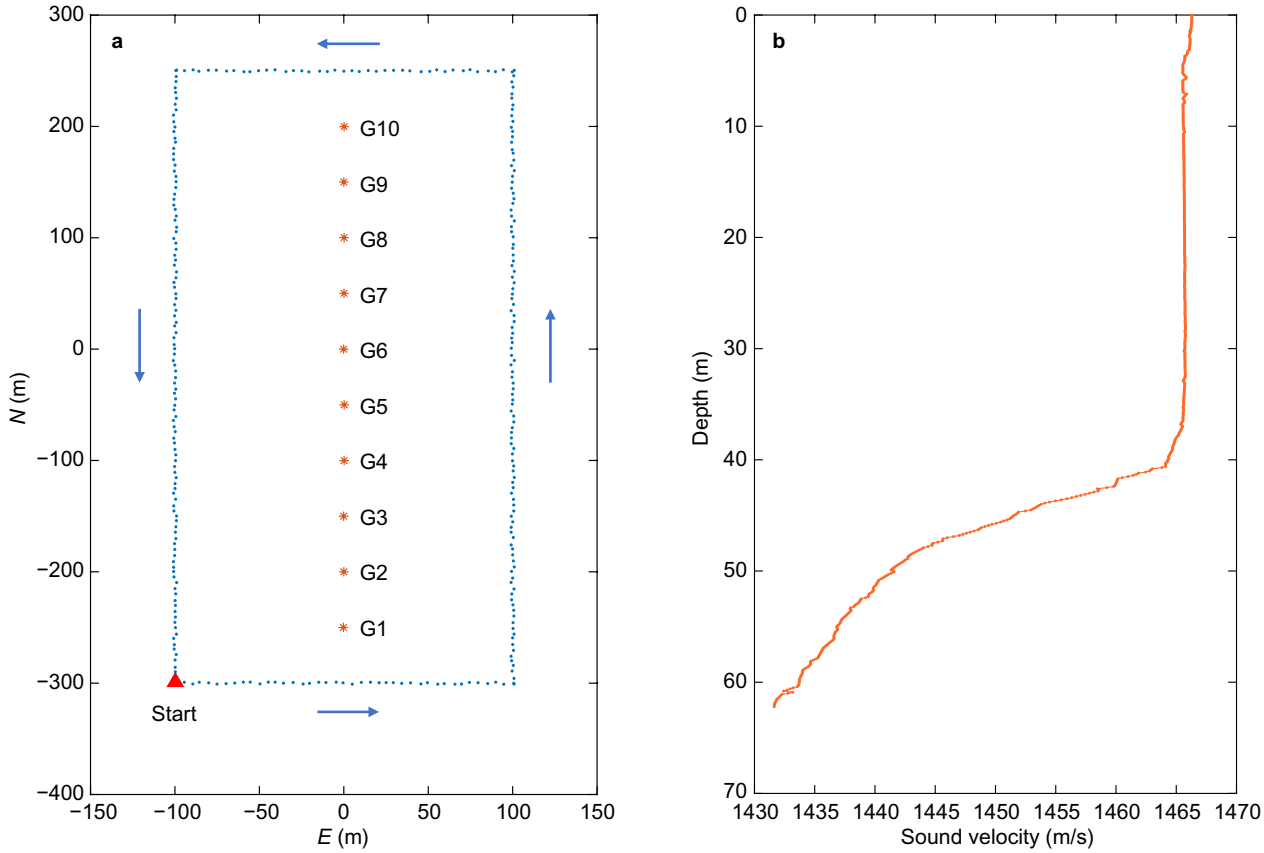

Fig. 5 **a** The simulated trajectory of the seismic survey ship. The red triangle indicates the starting position, and the blue arrow indicates the direction of sailing; **b** The SVP used in the simulation experiment

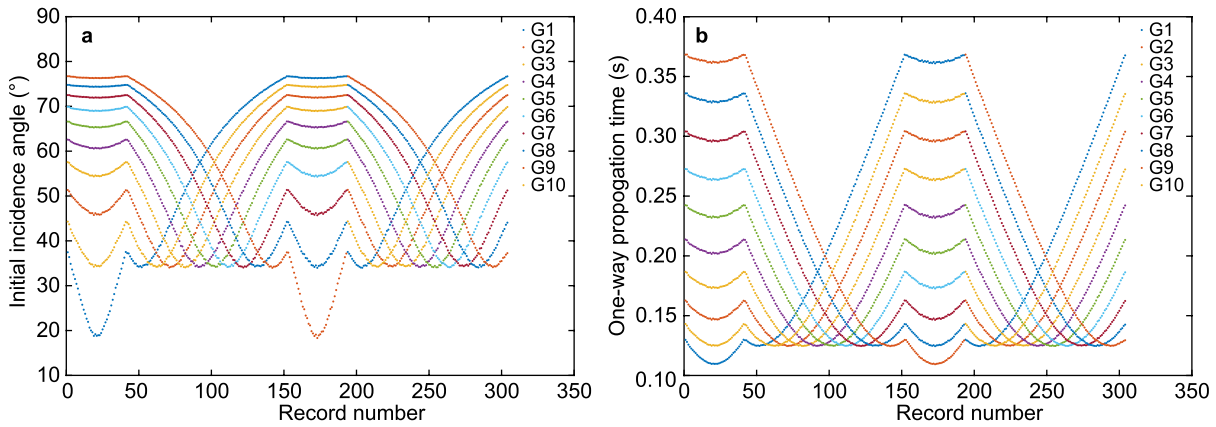

Fig. 6 The result of the inverse operation of acoustic ray tracing. **a** The theoretical initial incidence angle (unit: degree); **b** The one-way propagation time (unit: second)

tioning model in method 4 maintains an accuracy of 10 cm, with coordinate differences remaining around 20 cm.

(3) After introducing outliers to the original acoustic observations, the positioning accuracy of the basic acoustic positioning model in method 5 diminishes significantly, exceeding 1 m. and the coordinate

Table 2 The statistical result of the differences between the acoustic ray tracing results and the actual values. "Ave" is the symbol of the average value, "Std" is the symbol of the standard deviation

Point name	ΔZ (m)		ΔD (m)		ΔS (m)	
	Ave	Std	Ave	Std	Ave	Std
G1	0.111	0.103	0.041	0.028	0.041	0.028
G2	0.110	0.105	0.043	0.029	0.042	0.029
G3	0.115	0.106	0.040	0.030	0.047	0.031
G4	0.094	0.085	0.041	0.031	0.046	0.030
G5	0.095	0.077	0.041	0.029	0.042	0.029
G6	0.099	0.075	0.042	0.030	0.043	0.029
G7	0.101	0.078	0.040	0.029	0.043	0.031
G8	0.095	0.075	0.043	0.029	0.043	0.029
G9	0.094	0.084	0.042	0.029	0.045	0.029
G10	0.112	0.102	0.042	0.030	0.045	0.029

Table 3 The methods employed to determine the coordinates of geophones

Method	Model	SVP	C_0 (m/s)	Acoustic observations	Ratio of outliers	Outlier detection	Data buffer
1	Basic	Known	/	Ray tracing	/	/	/
2	SQ	Known	/	Ray tracing	/	$\alpha = 0.025$	15
3	Basic	Unknown	1466.30	Equation (19)	/	/	/
4	SQ	Unknown	1466.30	Equation (19)	/	$\alpha = 0.025$	15
5	Basic	Unknown	1466.30	Equation (19)	5%	/	/
6	Basic	Unknown	1466.30	Equation (19)	5%	$\alpha = 0.025$	/
7	SQ	Unknown	1466.30	Equation (19)	5%	$\alpha = 0.025$	15

differences reach the meter level. The positioning accuracy of the basic acoustic positioning model with Baarda's outlier detection in method 6 remains at a similar level as before, but the coordinate differences also reach the meter level. Conversely, the SQ positioning model in method 7 achieves an accuracy of approximately 10 cm, centimeter-level in most cases, and the coordinate differences are stable in about 20 cm.

The following conclusions can be drawn from Figs. 7, 8, and 9:

(1) It is evident from Fig. 7 that when the SVP is unknown, the coordinate differences between the geophone coordinates obtained by the SQ acoustic positioning method and the true values in the north direction are much smaller than those of the basic acoustic positioning model. When the SVP is known, the coordinate differences of the basic acoustic positioning model align with those of the SQ acoustic positioning method in the north direction. This suggests that the proposed method in this paper is more suitable for ocean bottom seismic exploration without SVPs.

(2) Figure 7 also reveals that the coordinate differences between the positioning result of the basic acoustic positioning model and the true values in the north direction are related to the location of geophones. Geophones G5 and G6 exhibit smaller coordinate differences in the north direction as they are in the center of the trajectory. However, no similar trend appears in the SQ acoustic positioning method, indicating that the proposed method has a wider scope of application.

(3) Figure 8 demonstrates that the coordinate differences among the methods in the east direction are consistently small. Additionally, the coordinate differences of the basic acoustic positioning model in the east direction are generally smaller than the differences in the north direction. This can be attributed to the smaller span of the track in the east–west direction compared to the north–south direction. Additionally, the incidence angles of acoustic waves change gradually when the sur-

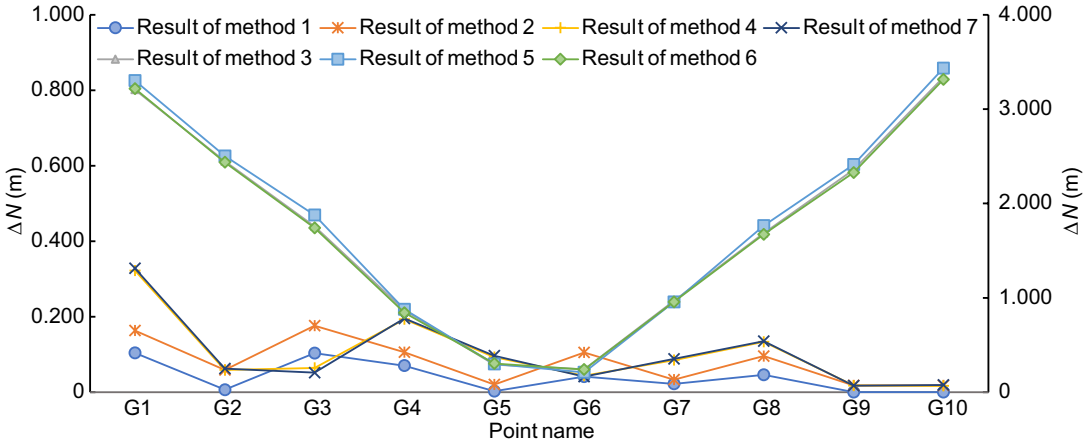

Fig. 7 The coordinate difference in the north direction between the coordinates of geophones calculated by method 1 to method 7 and the actual value. Method 3, method 5, and method 6 correspond to the secondary axis

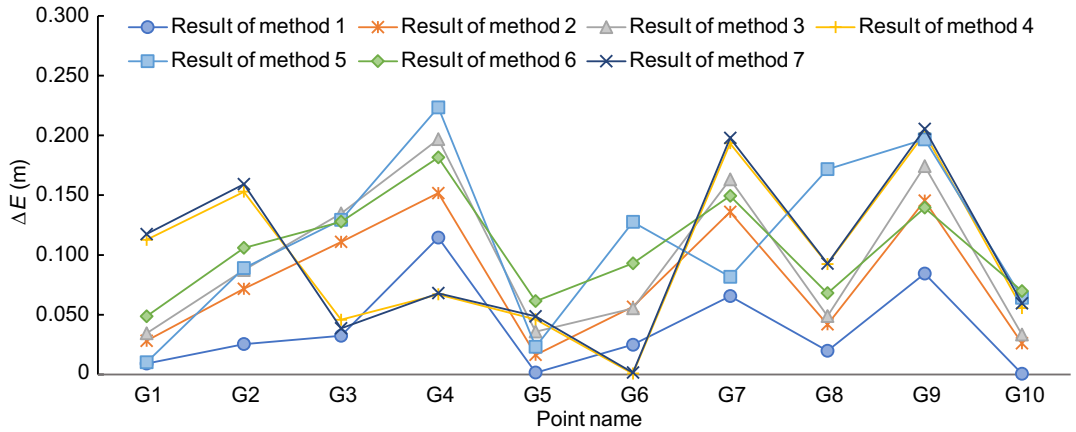

Fig. 8 The coordinate difference in the east direction between the coordinates of geophones calculated by method 1 to method 7 and the actual value

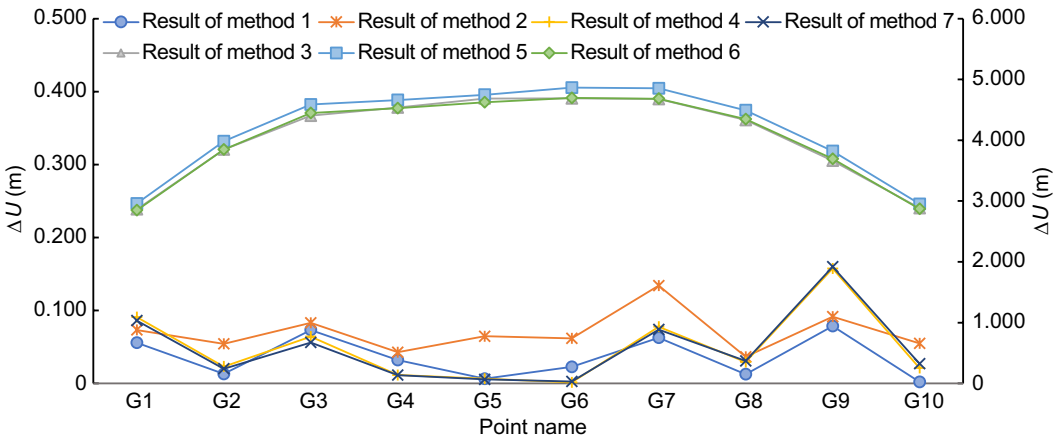

Fig. 9 The coordinate difference in the depth direction between the coordinates of geophones calculated by method 1 to method 7 and the actual value. method 3, method 5, and method 6 correspond to the secondary axis

Table 4 The posterior standard deviation of positioning models in method 1 to method 7

Point name	Standard deviation σ_1 of method 1 (m)	Standard deviation σ_2 of method 2 (m)	Standard deviation σ_3 of method 3 (m)	Standard deviation σ_4 of method 4 (m)	Standard deviation σ_5 of method 5 (m)	Standard deviation σ_6 of method 6 (m)	Standard deviation σ_7 of method 7 (m)
G1	0.007	0.006	0.192	0.216	1.146	0.195	0.224
G2	0.007	0.005	0.215	0.227	1.154	0.219	0.233
G3	0.009	0.010	0.237	0.212	1.133	0.241	0.199
G4	0.009	0.003	0.250	0.190	1.120	0.251	0.199
G5	0.004	0.002	0.256	0.128	1.039	0.257	0.131
G6	0.007	0.006	0.256	0.134	0.982	0.261	0.139
G7	0.008	0.003	0.250	0.113	0.980	0.256	0.114
G8	0.006	0.004	0.237	0.086	1.136	0.241	0.088
G9	0.009	0.005	0.214	0.064	1.090	0.217	0.068
G10	0.004	0.002	0.190	0.053	1.047	0.193	0.056

Table 5 The positioning errors in method 1 to method 7

Point name	Positioning error ΔP_1 of method 1 (m)	Positioning error ΔP_2 of method 2 (m)	Positioning error ΔP_3 of method 3 (m)	Positioning error ΔP_4 of method 4 (m)	Positioning error ΔP_5 of method 5 (m)	Positioning error ΔP_6 of method 6 (m)	Positioning error ΔP_7 of method 7 (m)
G1	0.118	0.181	4.300	0.353	4.435	4.298	0.359
G2	0.029	0.108	4.560	0.165	4.705	4.555	0.172
G3	0.131	0.224	4.744	0.102	4.959	4.777	0.085
G4	0.138	0.190	4.624	0.205	4.749	4.608	0.207
G5	0.007	0.070	4.696	0.104	4.758	4.637	0.108
G6	0.053	0.134	4.695	0.044	4.871	4.705	0.041
G7	0.093	0.194	4.780	0.225	4.948	4.782	0.229
G8	0.051	0.111	4.648	0.165	4.830	4.660	0.167
G9	0.115	0.173	4.360	0.256	4.523	4.369	0.261
G10	0.002	0.063	4.411	0.062	4.529	4.386	0.068

vey ship sails in the east–west direction, resulting in similar quality of acoustic observations within the same group. Conversely, the incidence angle changes drastically when the survey ship moves in the north–south direction.

(4) Figure 9 illustrates that the differences between the geophone coordinates calculated by the SQ acoustic positioning method in this paper and the actual values in the depth direction are considerably smaller than those of the basic acoustic positioning model, which greatly improves the positioning accuracy of the basic acoustic positioning model in the depth direction.

(5) Method 1, method 3, method 5, and method 6 are all based on the basic acoustic positioning model, which uses all original acoustic observations. On the other hand, method 2, method 4, and method 7 utilize the SQ acoustic positioning model, which involves grouping the acoustic observations before establishing the positioning model. A comprehensive comparison of method 1 to method 7 reveals that, except for method 1, which relies on accurate acoustic ray-tracing results, the basic acoustic positioning model exhibits lower accuracy compared to the SQ acoustic positioning model. Furthermore, the positioning error of the basic acoustic positioning model is significantly larger than that of the SQ acoustic positioning model achieving decimeter or centimeter level. This discrepancy can be attributed to the fact that the SQ acoustic positioning model distinguishes acoustic observations based on their incidence angles, thereby enhancing the utilization of high-quality observations obtained at smaller incidence angles.

The above experimental results can prove the robustness and accuracy of the SQ acoustic positioning method proposed in this paper.

Field experiment

To assess the practicability of the proposed method in the actual ocean bottom seismic exploration, an experiment was carried out using the data in a field survey conducted in the Bohai Sea, China on April 25, 2012. The field experiment was carried out on the 516 fleet of BGP INC., China National Petroleum Corporation. The acoustic positioning system is BPS developed by BGP INC., including four parts: master machine, transducer, encoder, and transponder (Fig. 10). The transmitting sound source level of the transducer and transponder is 185 dB and their receiving sensitivity is −195 dB. The frequency of sound waves is 34–50 kHz.

The area of the field survey is shown in Fig. 11a, with a water depth of about 15 m. A total of 19 acoustic transponders were deployed to the sea bottom, and three of them were performed the circle-sailing positioning. The sailing trajectory and the design positions of seafloor transponders are given in Fig. 11b.

The number of original acoustic observations (the one-way propagation time of acoustic wave) corresponding to each seafloor transponder is given in Fig. 12. The incidence angle calculated by Eq. (19) and the observed one-way propagation time of acoustic wave are given in Fig. 13.

As can be seen from Fig. 13, the shallow water depth results in large initial incidence angles of the acoustic waves, with some angles even approaching 90 degrees. Additionally, there are outliers in the observed one-way propagation time. Because of the fast-sailing speed of the survey ship, the initial incidence angles change rapidly, for which the data buffer size of the SQ acoustic positioning method should be reduced. It is worth noting that a minimum of three observations is required to calculate the coordinates of the geophone. Therefore, to ensure the redundancy of the acoustic positioning model and consistency in the quality of observations within the same group, the data buffer size is set to 5 in this experiment.

Since the SVP of the water was not collected during the field survey, only the basic acoustic positioning model in method 3 and the SQ acoustic positioning model in method 4 were used to determine the coordinates of the 19 seafloor transponders, in which the sound velocity on the sea surface is 1452.70 m/s. The posterior standard variance of the two models is shown in Fig. 14.

As depicted in Fig. 14, the posterior standard deviation of the basic acoustic positioning model is 0.5 m approximately, while that of the SQ acoustic positioning model is much smaller, less than 0.1 m. It is evident that the more observations, the higher the accuracy of the proposed method, and the greater the accuracy improvement compared with the basic acoustic positioning model. Therefore, in the field survey, it is advisable to increase the number of observations.

Taking the results of circle-sailing positioning as the reference, the differences between the coordinates of transponders obtained by the two models and the results of circle-sailing positioning are given in Table 6, where "ΔP" represents the positioning error and equal to the quadratic root of the sum of squares of ΔN, ΔE and ΔU.

Table 6 reveals that the positioning error between the SQ acoustic positioning model and the circle-sailing positioning are smaller than those of the basic acoustic positioning model, indicating the high accuracy of the proposed method. The primary disparity between the basic acoustic positioning and the circle-sailing positioning lies in the depth direction, aligning with the notion that the accuracy of the basic acoustic positioning model in the depth direction is relatively low. In conclusion, the proposed method proves to be effective and practical in ocean bottom seismic exploration.

To verify the influence of the data buffer size on positioning results, the field experiment was repeated with the data buffer size of 4, 6, 7, and 8, respectively. The posterior standard deviations of the SQ acoustic positioning method under different data buffer sizes are shown in Fig. 15.

From Fig. 15, it can be observed that when the data buffer size is set to 7 and 8, the posterior standard deviations of G15 and G17 exceed 1 m. Conversely, the

Fig. 10 The BPS acoustic positioning system: **a** master machine, **b** transducer, **c** encoder, **d** transponder

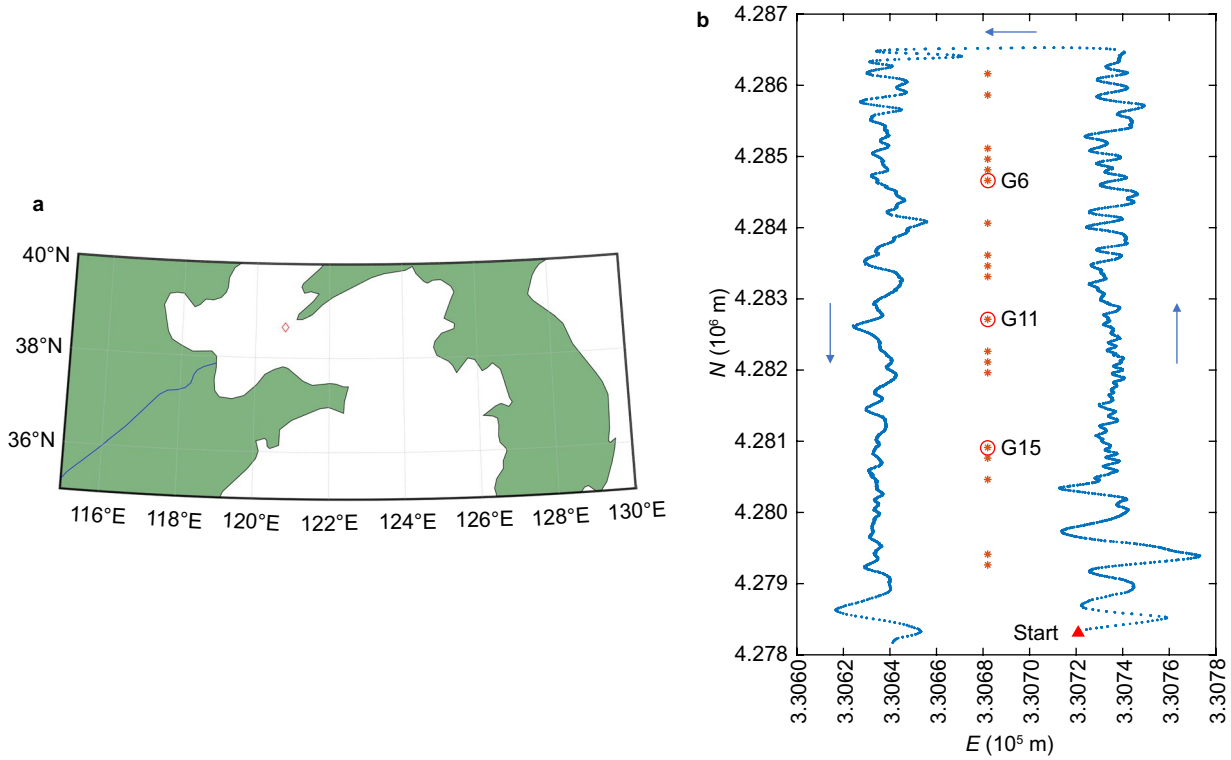

Fig. 11 **a** The sea area of the field survey (the red diamond indicates the starting point of the survey ship). **b** The sailing trajectory and the design position of seafloor transponders (the red triangle indicates the starting position, and the blue arrow indicates the direction of sailing; the red circle indicates the transponder performed the circle-sailing positioning)

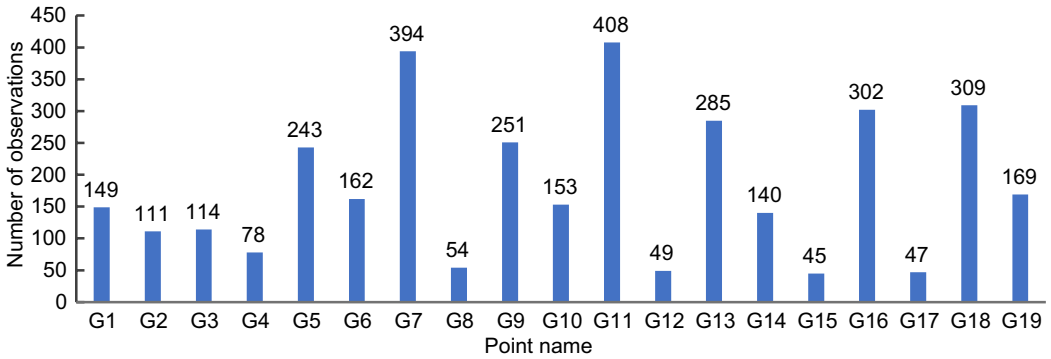

Fig. 12 The number of the observed one-way propagation time of acoustic waves

posterior standard deviations of the other geophones remain at the centimeter level with small variation. To understand the significant fluctuations in the posterior standard deviations of G15 and G17, it was analyzed in conjunction with Fig. 12. It was discovered that there were only 45 and 47 observations for G15 and G17, respectively, and the collections of these observations were not continuous, for which the data quality within the same group becomes more pronounced when the data buffer size is larger. This finding validates the rationality of setting the data buffer size based on the speed of the ship.

Discussion

Comparison with a similar method

In 2019, a multi-objective sequential solution method was proposed (Liu et al., 2019), which sets threshold values according to the incidence angle of acoustic

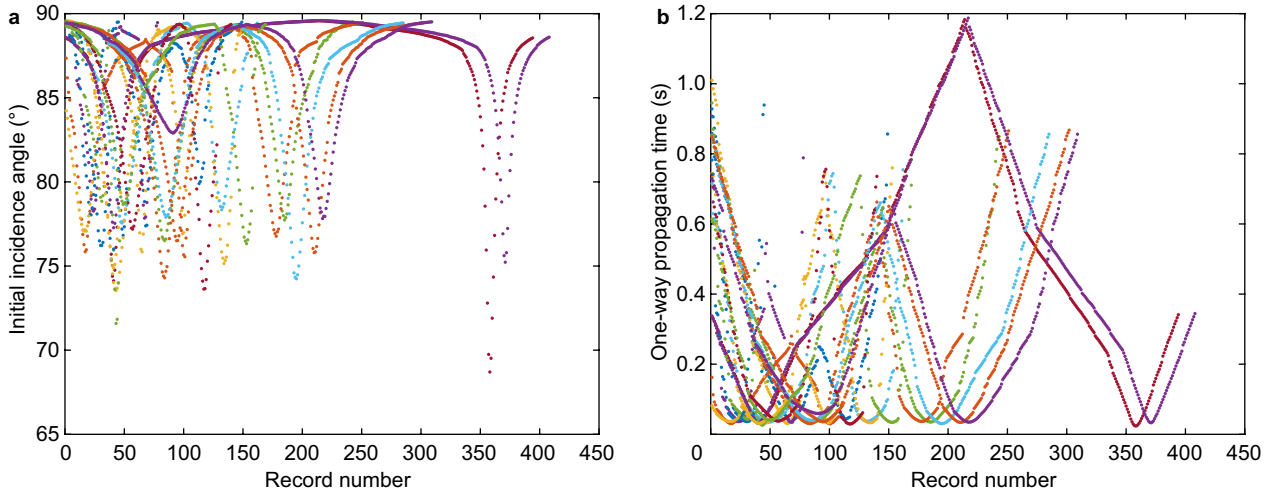

Fig. 13 **a** The initial incidence angle calculated by Eq. (19) (unit: degree); **b** The observed one-way propagation time (unit: second)

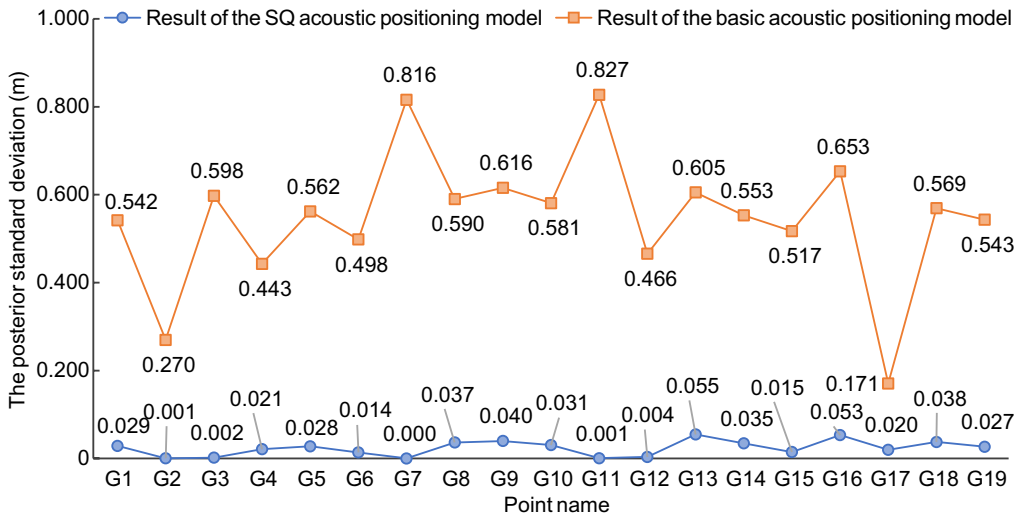

Fig. 14 The posterior standard deviation of the basic acoustic positioning model and the SQ acoustic positioning model (unit: meter)

waves and solves the correction values of acoustic ranging results in different incidence angle intervals based on sequential adjustment, including two models of parametric (called "US(B) model" for short) and modeling (called "US(M) model" for short) of sound line bending. In this section, the data from simulation experiments will be used to compare the US(B) model, the US(M) model, and the proposed method. In the US(B) model

Table 6 The coordinate differences between the basic acoustic positioning model, the SQ acoustic positioning model and the circle-sailing positioning

Point name	Results of the basic acoustic positioning model (m)				Results of the SQ acoustic positioning model (m)			
	ΔN	ΔE	ΔU	ΔP	ΔN	ΔE	ΔU	ΔP
G6	0.040	0.041	0.286	0.292	0.061	0.102	0.061	0.134
G11	0.050	0.068	0.315	0.326	0.058	0.093	0.023	0.112
G15	0.021	0.030	0.427	0.429	0.064	0.109	0.220	0.254

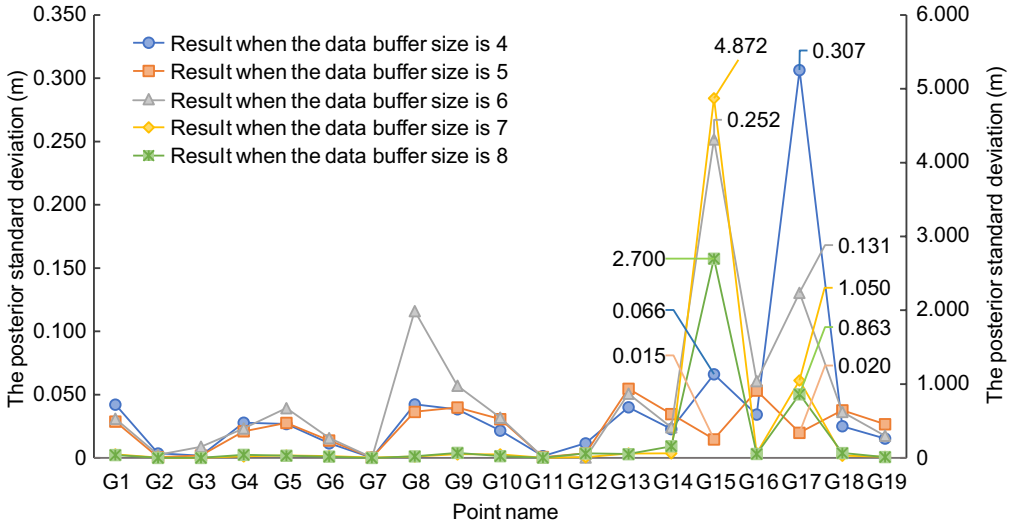

Fig. 15 The posterior standard deviation of the SQ acoustic positioning model under different data buffer sizes, where the data buffer size 7 and 8 correspond to the secondary vertical axis. (unit: meter)

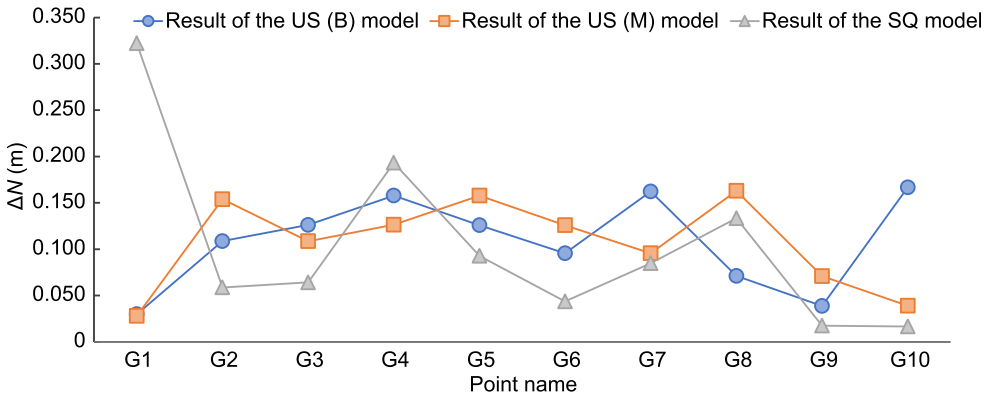

Fig. 16 The coordinate difference in the north direction between the coordinates of geophones calculated by the US(B) model, the US(M) model, and the SQ acoustic positioning model

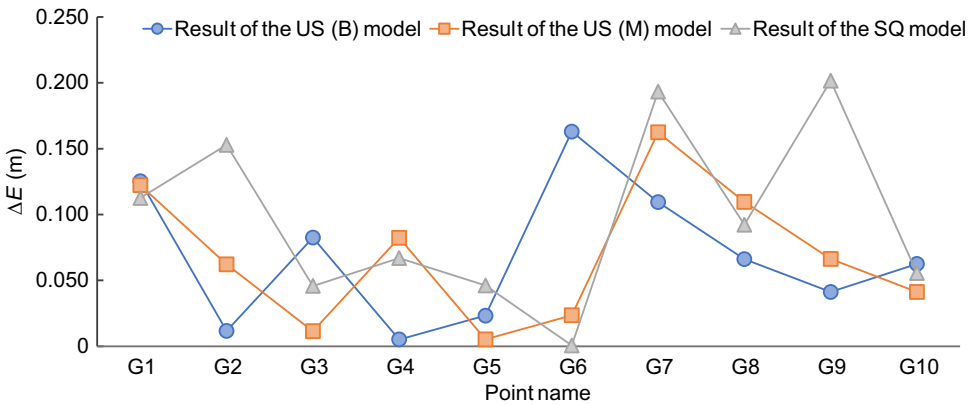

Fig. 17 The coordinate difference in the east direction between the coordinates of geophones calculated by the US(B) model, the US(M) model, and the SQ acoustic positioning model

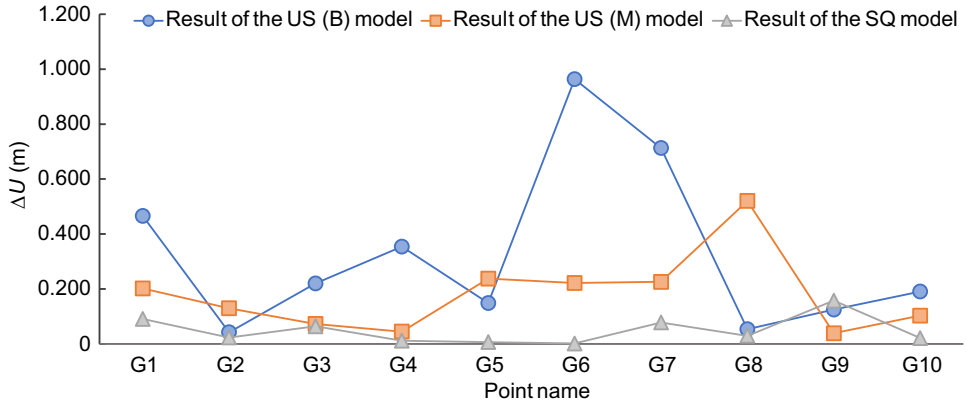

Fig. 18 The coordinate difference in the depth direction between the coordinates of geophones calculated by the US(B) model, the US(M) model, and the SQ acoustic positioning model

and US(M) model, the incidence angles of sound waves are grouped by 1°. The differences between the geophone coordinates obtained with each method and the actual value are shown in Figs. 16, 17, 18. The posterior standard deviations and positioning errors corresponding to the three methods are given in Table 7.

As can be seen from Table 7, compared with the traditional acoustic positioning model, the positioning accuracy with the US(B) model and the US(M) model is greatly improved. Overall, the accuracy with the US(M) model and the SQ acoustic positioning model is comparable, and the two models are more accurate than the US(B) model. It can be seen from Figs. 16, 17, 18 that the positioning errors of horizontal coordinates of the three models are similar, but the positioning error of the SQ acoustic positioning model is smaller than that of the US(B) and US(M) models in the depth direction.

In addition, the US(B) and US(M) models use all the observations corresponding to each geophone, and the object of sequential adjustment is to get the corrections of the acoustic ranging results in different incidence angle intervals. The SQ acoustic positioning model takes in the observations in the preset data buffers of each geophone, and the object of sequential adjustment is to get the coordinates of geophones. The three models can improve the efficiency of data resolution, but the differences in their principles lead to different usage scenarios. The SQ acoustic positioning model can be used for real-time positioning of geophones in the measurement process, while US(B) and US(M) models are suitable for fine processing in data post-processing.

The range of incidence angles of high-precision acoustic ranging in different water depths

In different water depths, the distance calculation error, which refers to the discrepancies between the geometric distance calculated using the sound velocity on the sea surface and the results obtained through acoustic ray tracing, varies significantly. The range of incidence angles corresponding to the smaller distance calculation errors, known as the "suitable incidence angle interval", differs across different water depths. When an initial incidence angle exceeds the suitable incidence angle interval, the large distance calculation error lowers the accuracy of acoustic positioning. Therefore, it is necessary to set a suitable incidence angle interval, beyond which acoustic observations will not be included in the acoustic positioning model. Figure 19 depicts the relationship between the initial incident angle of acoustic waves and the distance calculation error in different water depths.

As depicted in Fig. 19, it is evident that under the same water depth, a larger initial incidence angle of the acoustic wave corresponds to a greater distance calculation error. Similarly, at the same incident angle, the distance calculation error increases with deeper water depths. To eliminate the acoustic observations with large distance calculation errors, it is necessary to predefine the acoustic data acquisition range of the survey ship by considering both the ranging accuracy and water depth. Set the water depth as D and begin to collect acoustic observations when the distance between the seismic geophones and the survey ship is S. Firstly, the appropriate interval of incidence angle $[\theta_1, \theta_2]$ under the current water depth can be determined based on the ranging accuracy requirements. For example, at a water depth of 500 m, if the relative distance calculation error should be less than 5%, implying the distance calculation error should be less than 25 m, the appropriate interval of incidence angle should be set to [10°, 60°] according to Fig. 19, and then the acoustic data acquisition range S can be obtained according to Eq. (29).

$$D/\tan\theta_2 \le S \le D/\tan\theta_1 \tag{29}$$

The applicable water depth of the SQ acoustic positioning method

The positioning accuracy of the SQ acoustic positioning method under varying water depths is given in Fig. 20. As can be seen from Fig. 20, when the water depth is less than 5 m, the positioning accuracy of the SQ acoustic positioning method is low. However, when the water depth is about 30 m, the positioning accuracy reaches its peak, achieving centimeter-level precision. As the water depth increases, the positioning accuracy decreases gradually. Beyond a water depth of 200 m, the positioning accuracy falls below 0.2 m, and for water depths exceeding 400 m, the accuracy drops below 0.5 m.

In summary, the SQ acoustic positioning method exhibits high accuracy for the water depth ranging from 30 to 200 m, the most suitable range for the proposed method in this study. For water depths below 5 m or exceeding 400 m, the positioning accuracy with the proposed method is lower than 0.5 m. In such cases, the acoustic positioning and first break positioning can be combined to accurately locate the geophone.

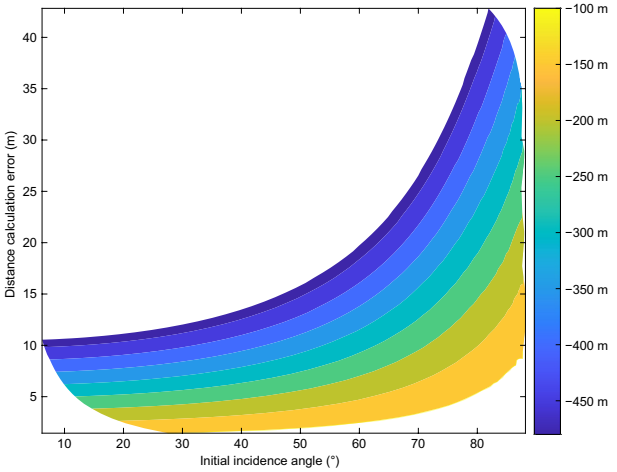

Fig. 19 The relationship between the initial incident angle and the distance calculation error in different water depths (different colors represent different water depths)

Conclusion

Addressing the limitations of the current acoustic positioning method for seismic geophones, such as ineffective outlier removal in acoustic observations, incomplete utilization of high-precision data, and low computational efficiency, this paper proposes a rigorous real-time acoustic positioning method for geophones.

In the proposed method, the acoustic observations are grouped first to establish the intra-group positioning model. To effectively identify and eliminate outliers in the acoustic observations, an outlier detection algorithm is incorporated in the solution of the intra-group positioning model. By adjusting the weight of observations, the proportion of positioning results

Table 7 The posterior standard deviations and positioning errors of the US(B) model, the US(M) model, and the SQ acoustic positioning model

Point name	Results of US(B) model (m)		Results of US(M) model (m)		Results of SQ model (m)	
	σ_B	ΔP_B	σ_M	ΔP_M	σ_{SQ}	ΔP_{SQ}
G1	0.089	0.483	0.033	0.238	0.216	0.353
G2	0.105	0.117	0.018	0.211	0.227	0.165
G3	0.235	0.267	0.049	0.131	0.212	0.102
G4	0.374	0.387	0.118	0.157	0.190	0.205
G5	0.467	0.196	0.216	0.285	0.128	0.104
G6	0.525	0.982	0.289	0.256	0.134	0.044
G7	0.367	0.739	0.297	0.294	0.113	0.225
G8	0.144	0.111	0.202	0.556	0.086	0.165
G9	0.073	0.137	0.072	0.105	0.064	0.256
G10	0.064	0.261	0.034	0.117	0.053	0.062

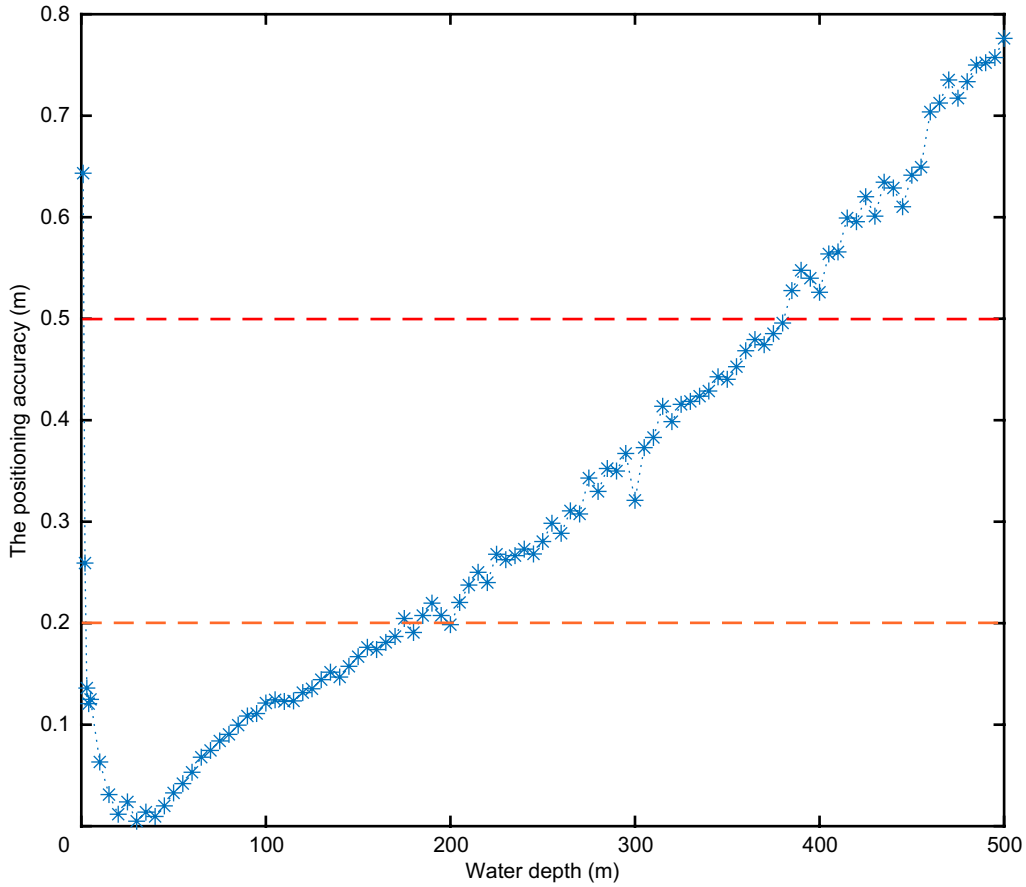

Fig. 20 The positioning accuracy of SQ acoustic positioning method under different water depths (unit: meter)

using high-quality data groups is increased while the proportion using low-quality data groups is reduced. This approach effectively avoids wasting high-quality observations by mixing them with all observations in the establishment of the positioning model. In addition, only the positioning results of the previous data group need to be stored, alleviating memory pressure. It is proved by experiments that the proposed method is effective and practical in seafloor seismic exploration. Experimental results demonstrate that the proposed method can achieve centimeter-level positioning accuracy, with a positioning error of approximately 20 cm in the absence of SVPs.

Appendix

Substituting Eq. (14) into the first formula in Eq. (13), we can obtain Eq. (30).

$$dy = \sum_{i=1}^{n} \tan\theta_i d(\Delta z_i) + C_0^2 \cos\theta_0 \left(\sum_{i=1}^{n} \frac{\Delta z_i C_i}{\sqrt{\left(C_0^2 - C_i^2 \sin^2\theta_0\right)^3}} \right) d\theta_0 \tag{30}$$

By differentiating Eq. (11), we can obtain Eq. (31).

$$dS = \frac{ydy + zdz}{\sqrt{y^2 + z^2}} \tag{31}$$

Then, Eq. (32) can be obtained by substituting Eq. (13) and (30) into Eq. (31).

$$dS = \frac{y}{\sqrt{y^2 + z^2}} \left\{ \sum_{i=1}^{n} \tan\theta_i d(\Delta z_i) + C_0^2 \cos\theta_0 \left(\sum_{i=1}^{n} \frac{\Delta z_i C_i}{\sqrt{\left(C_0^2 - C_i^2 \sin^2\theta_0\right)^3}} \right) d\theta_0 \right\} + \frac{z}{\sqrt{y^2 + z^2}} \sum_{i=1}^{n} d(\Delta z_i) \tag{32}$$

Since the height of each layer of the SVP is known, that is, $d(\Delta z_i)$ is equal to zero, Eq. (32) can be simplified as Eq. (33).

$$dS = \frac{yC_0^2 \cos\theta_0}{\sqrt{y^2+z^2}} \left(\sum_{i=1}^{n} \frac{\Delta z_i C_i}{\sqrt{\left(C_0^2 - C_i^2 \sin^2\theta_0\right)^3}} \right) d\theta_0 \tag{33}$$

Based on the law of variance propagation, the relation between the accuracy of acoustic ranging σ_S and the accuracy of the initial incidence angle σ_{θ_0} can be obtained, as shown in Eq. (15).

Acknowledgements
Not applicable.

Author contributions
JM: Conceptualization, Methodology, Data curation, Validation, Writing—original draft, Writing—review & editing. SF: Conceptualization, Writing—review & editing. JZ: Conceptualization, Writing—review & editing.

Funding
This research is supported by the National Key R&D Program of China (Grant No.: 2016YFB0501703) and Science and Technology Innovation Project (Grant No.: LSKJ202205102) Funded by Laoshan Laboratory.

Data availability
The datasets and source code generated or analyzed during the current study are freely available at an online GitHub git repository upon request to the corresponding author.

Declarations

Competing interests
The authors declare that they have no known competing interests or personal relationships that could have appeared to influence the work reported in this paper.

Received: 14 April 2023 Accepted: 21 November 2023
Published online: 19 February 2024

References

Alghamdi, A., Mingzhong, H., Aldeghaither, S., Khan, A., Alzahrani, S., Tsingas, C., Donliang, Z., & Diallo, M. S. (2018). Processing challenges and technologies of ocean-bottom node survey. In *SEG Technical Program Expanded Abstracts 2018, SEG Technical Program Expanded Abstracts. Society of Exploration Geophysicists* (pp. 4060–4064). https://doi.org/10.1190/segam2018-2995816.1

Baarda, W. (1968). *A testing procedure for use in geodetic networks*. Netherlands Geodetic Commission.

Baarda, W. (1967). *Statistical concepts in geodesy*. Netherlands Geodetic Commission.

Barr, F. J. (1994). Ocean-bottom cable use surges for seismic data acquisition. *Oil and Gas Journal 92*, 43.

Barr, F. J., Paffenholz, J., Rabson, W. (1996). The dual-sensor ocean-bottom cable method: Comparative geophysical attributes, quantitative geophone coupling analysis and other recent advances. In: *SEG Technical Program Expanded Abstracts 1996, SEG Technical Program Expanded Abstracts* (pp. 21–23). Society of Exploration Geophysicists. https://doi.org/10.1190/1.1826602

Berg, E., Svenning, B., Martin, J. (1994). SUMIC: Multicomponent sea-bottom seismic surveying in the North Sea—Data interpretation and applications. In *SEG Technical Program Expanded Abstracts 1994, SEG Technical Program Expanded Abstracts* (pp. 477–480). Society of Exploration Geophysicists. https://doi.org/10.1190/1.1932132

BGP INC., C.N.P.C. (2016). *BPS Acoustic Positioning System [WWW Document]*. http://www.bgp.com.cn/bgpen/SoftwareDevelopment/201610/0edbe87817a94d1fad2c06e284624be1.shtml. Accessed December 4, 2023.

Bianco, M., & Gerstoft, P. (2017). Dictionary learning of sound speed profiles. *Journal of the Acoustical Society of America, 141*, 1749–1758. https://doi.org/10.1121/1.4977926

Bole, J., & Zinn, N. (1998). Seismic detector positioning in a 4D/4C OBC survey using both acoustics and first breaks. *First Break, 17*, 305–309. https://doi.org/10.3997/2214-4609.201408117

Bovet, L., Ceragioli, E., Tchikanha, S., Guilbot, J., & Toinet, S. (2010). Ocean Bottom Nodes Processing: reconciliation of Streamer and OBN data sets for Time Lapse Seismic Monitoring. The Angolan Deep Offshore Experience. In *SEG Technical Program Expanded Abstracts 2010, SEG Technical Program Expanded Abstracts* (pp. 3751–3755). Society of Exploration Geophysicists. https://doi.org/10.1190/1.3513630

Clarke, J. E. H., Lamplugh, M., & Kammerer, E. (2000). Integration of near-continuous sound speed profile information. *Can. Hydrogr. Conf.*

Cui, X., Yu, Z., Tao, B., Liu, D., Yu, Z. L., Sun, H., & Wang, X. (2015). Sequential static filtering. In *The Principle of Generalized Surveying Adjustment*. Wuhan University Press (pp. 78–84).

Detomo, R., Quadt, E., Pirmez, C., Mbah, R., & Olotu, S. (2012). Ocean Bottom Node Seismic: Learnings from Bonga, Deepwater Offshore Nigeria. In *SEG Technical Program Expanded Abstracts 2012, SEG Technical Program Expanded Abstracts* (pp. 1–5). Society of Exploration Geophysicists. https://doi.org/10.1190/segam2012-0583.1

Ding, J., Zhou, X., Tang, Q., & Chen, Y. (2007). Expression of multi-beam echo sounding sound velocity profile with empirical orthogonal functions. *Geomatics and Information Science of Wuhan University, 32*, 446–449.

Fang, S. (2014). *Research on key technique of navigation and positioning in ocean bottom cable seismic operation and system development*. Wuhan university.

Fujita, M., Ishikawa, T., Mochizuki, M., Sato, M., Toyama, S., Katayama, M., Kawai, K., Matsumoto, Y., Yabuki, T., Asada, A., & Colombo, O. L. (2006). GPS/Acoustic seafloor geodetic observation: Method of data analysis and its application. *Earth, Planets and Space, 58*, 265–275. https://doi.org/10.1186/BF03351923

Huang, J., Luo, Y., Li, Y., Shi, J., Zheng, X., & Wang, J., 2021. Analysis of Sound Speed Profile in the South China Sea based on Empirical Orthogonal Function Algorithm. In: 2021 OES China Ocean Acoustics (COA). pp. 166–171. https://doi.org/10.1109/COA50123.2021.9520009

LeBlanc, L. R., & Middleton, F. H. (1980). An underwater acoustic sound velocity data model. *Journal of the Acoustical Society of America, 67*, 2055–2062. https://doi.org/10.1121/1.384448

Lecerf, D., Lafram, A., Boelle, J.-L., & Cantillo J. (2011). Ocean Bottom Node processing in deep offshore environment for reservoir monitoring. In *12th International Congress of the Brazilian Geophysical Society & EXPOGEF, Rio de Janeiro, Brazil, 15–18 August 2011, SEG Global Meeting Abstracts* (pp. 2095–2098). Brazilian Geophysical Society. https://doi.org/10.1190/sbgf2011-435

Li, H., Jiang, X., & Li, Z. (2004). Robust estimation in Gaussian filtering for engineering surface characterization. *Precision Engineering, 28*, 186–193. https://doi.org/10.1016/j.precisioneng.2003.10.004

Li, T., Zhao, J., & Ma, J. (2022). A precise underwater positioning method by considering the location difference of transmitting and receiving sound waves. *Ocean Engineering, 247*, 110480. https://doi.org/10.1016/j.oceaneng.2021.110480

Li, Z., He, L., Zhang, R., Li, F., Yu, Y., & Lin, P. (2015). Sound speed profile inversion using a horizontal line array in shallow water. *Science China Physics, Mechanics & Astronomy, 58*, 1–7. https://doi.org/10.1007/s11433-014-5526-x

Liu, H., Yu, Z., Wu, S., Chen, Y., Zhang, H., Zhao, S. (2019). A positioning determination of multi-transponders with sound ray bending in shallow waters. *Oil Geophysics Prospectives 54*, 9–15. https://doi.org/10.13810/j.cnki.issn.1000-7210.2019.01.002

Medwin, H., Clay, C. S. (1998). Chapter 3—Transmissions Along Ray Paths. In Medwin, H., Clay, C. S. (Eds.) *Fundamentals of Acoustical Oceanography, Applications of Modern Acoustics* (pp. 70–126). Academic Press, San Diego. https://doi.org/10.1016/B978-012487570-8/50005-2

Morvan, P.-Y., Pelletier, H., Blomme, R., 2015. Positioning for Ocean Bottom Systems (OBS) applications: A case study, in: 2015 IEEE/OES Acoustics in

Underwater Geosciences Symposium (RIO Acoustics). Presented at the 2015 IEEE/OES Acoustics in Underwater Geosciences Symposium (RIO Acoustics), pp. 1–4. https://doi.org/10.1109/RIOAcoustics.2015.7473646
Munk, W., & Wunsch, C. (1979). Ocean acoustic tomography: A scheme for large scale monitoring. *Deep Sea Research Part A. Oceanographic Research Papers*, *26*, 123–161. https://doi.org/10.1016/0198-0149(79)90073-6
Osada, Y., Fujimoto, H., Miura, S., Sweeney, A., Kanazawa, T., Nakao, S., Sakai, S., Hildebrand, J. A., & Chadwell, C. D. (2003). Estimation and correction for the effect of sound velocity variation on GPS/Acoustic seafloor positioning: An experiment off Hawaii Island. *Earth, Planets and Space, 55*, e17–e20. https://doi.org/10.1186/BF03352464
Park, J. C., & Kennedy, R. M. (1996). Remote sensing of ocean sound speed profiles by a perceptron neural network. *IEEE Journal of Oceanic Engineering, 21*, 216–224. https://doi.org/10.1109/48.486796
Sakic, P., Ballu, V., Crawford, W. C., & Wöppelmann, G. (2018). Acoustic ray tracing comparisons in the context of geodetic precise off-shore positioning experiments. *Marine Geodesy, 41*, 315–330. https://doi.org/10.1080/01490419.2018.1438322
Sakic, P., Ballu, V., & Royer, J.-Y. (2020). A Multi-observation least-squares inversion for gnss-acoustic seafloor positioning. *Remote Sensing, 12*, 448. https://doi.org/10.3390/rs12030448
Sonardyne (2021). *TZ/OBC - Seismic Positioning Beacon - Datasheets - Sonardyne [WWW Document]*. https://www.sonardyne.com/products-knowledge-base/tz-obc-seismic-positioning-beacon-datasheets/. Accessed December 4, 23.
Sun, W., Bao, J., Jin, S., Xiao, F., & Cui, Y. (2016). Inversion of Sound Velocity Profiles by Correcting the Terrain Distortion. *Geomatics and Information Science of Wuhan University,* 41, 349–355. https://doi.org/10.13203/j.whugis20140142
Wang, X., Tao, B., Qiu, W., & Yao, Y. (2014). *Advanced Surveying Adjustment*. Surveying and Mapping Press.
Wang, X., Xue, S., Qu, G., Liu, Y., & Yang, W. (2021). Disturbance analysis of underwater positioning acoustic ray and design of piecewise exponential weight function. *Acta Geodaetica et Cartographica Sinica, 50*, 982–989.
Wang, Z., Li, S., Nie, Z., Wang, Y., Wu, S. (2016). A Large Incidence Angle Ray-Tracing Method for Underwater Acoustic Positioning. *Geomatics and Information Science of Wuhan University, 41*, 1404–1408. https://doi.org/10.13203/j.whugis20140626
Wang, Z., Zhou, H., Tong, S., Fang, Y., & Cao, G. (2020). Secondary positioning of deep ocean bottom nodes. *Oil Geophysical Prospecting, 55*, 242–247. https://doi.org/10.13810/j.cnki.issn.1000-7210.2020.02.002
Zeng, X., & Yang, W. (2001). Brief analysis of secondary positioning system in seismic sea-bottom cable acquisition. *Oil Geophysical Prospecting, 36*, 220–226.
Zhang, D., Tsingas, C., Ghamdi, A., Huang, M., Jeong, W., Sliz, K., Aldeghaither, S., & Zahrani, S. (2021). A review of OBN processing: Challenges and solutions. *Journal of Geophysics and Engineering, 18*, 492–502. https://doi.org/10.1093/jge/gxab024
Zhao, J., Chen, X., Zhang, H., & Feng, J. (2018). Localization of an Underwater Control Network Based on Quasi-Stable Adjustment. *Sensors, 18*. https://doi.org/10.3390/s18040950
Zhao, J., & Liang, W. (2019). Some key points of submarine control network measurement and calculation. *Acta Geodaetica et Cartographica Sinica, 48*, 1197–1202. https://doi.org/10.11947/j.AGCS.2019.20190157
Zhao, J., Liang, W., Ma, J., Liu, M., & Li, Y. (2023). A Self-Constraint Underwater Positioning Method without the Assistance of Measured Sound Velocity Profile. *Marine Geodesy, 46*, 62–82. https://doi.org/10.1080/01490419.2022.2079778
Zhao, S., Wang, Z., & Liu, H. (2018). Investigation on Underwater Positioning Stochastic Model Based on Sound Ray Incidence Angle. *Acta Geodaetica et Cartographica Sinica, 47*, 1280–1289. https://doi.org/10.11947/j.AGCS.2018.20170026
Zinn, N., 2011. Using Cross-Correlated, Head-Wave and Diving-Wave Seismic Energy to Position Ocean Bottom Seismic Cables [WWW Document]. Hydrom. 2010–2021. URL http://www.hydrometronics.com/downloads.html (accessed 4.12.23).
Zinn, N. (1998). Ocean-Bottom Cable Detector Positioning: Acoustics versus First Breaks. *The Hydrographic Journal, 87*, 26–34.

Publisher's Note